Pyruvate kinase M2 plays a pivotal role in promoting PD-L1 expression and malignant behaviors of hepatoma cells

Qiuyue Zhang[1], Kailin Huang[1], Junnv Xu[1,2], Xueqin Wu[1], Haifeng Lin[2], Bo Lin[1], Mingyue Zhu[1]*, Mengsen Li[1,2]*

[1]Key Laboratory of Tropical Translational Medicine, Ministry of Education, and Hainan Provincial Key Laboratory of Carcinogenesis and Intervention, Hainan Medical University, Haikou, Hainan Province, China
[2]Department of Medical Oncology, Second Affiliated Hospital, Hainan Medical University, Haikou, Hainan Province, China

Submitted: 21 January 2025; **Accepted:** 14 July 2025
Online publication: 23 August 2025

Arch Med Sci
DOI: https://doi.org/10.5114/aoms/208245

***Corresponding authors:**
Mengsen Li
Mingyue Zhu
Key Laboratory of Tropical Translational Medicine
Ministry of Education,
and Hainan Provincial
Key Laboratory of
Carcinogenesis and
Intervention
Hainan Medical University
3 Xueyuan Road
Longhua District
Hainan Medical University
Haikou 571199
Hainan, China
E-mail: mengsenli@163.com;
mingyuezhu2002@163.com

Abstract

Introduction: Pyruvate kinase M2 (PKM2) is a key rate-limiting enzyme that regulates glucose metabolic reprogramming (Warburg effect), but the correlation between PKM2 and PD-L1 or malignant behaviors in hepatocellular carcinoma (HCC) cells remains unknown. This study explored the role of PKM2 and the Warburg effect on the expression of PD-L1 and the malignant behaviors of HCC cells.

Material and methods: The relationship between the Warburg effect and key enzymes and signaling pathways was analyzed using bioinformatics; the expression of PD-L1, PKM2, and hexokinase 2 (HK2) in 30 patients' HCC tissues and paired para-cancerous tissues was detected by immunohistochemistry and Western blotting. Short hairpin RNA (shRNA) silencing the expression of PKM2 was used to explore its influence on the expression of PD-L1 in HCC cells. The malignant behaviors of HCC cells were detected by scratch test, plate cloning experiment, Transwell migration experiment, and EdU staining; the concentrations of lactic acid, pyruvate, and ATP and the consumption of glucose were detected using a reagent kit.

Results: Biological information database and detection of HCC tissues and paired para-cancerous tissues showed that the expression levels of PKM2 and PD-L1 were significantly higher in HCC tissues than in paired para-cancerous tissues, and the expression of PKM2 was positively correlated with PD-L1 expression. PKM2 could promote the proliferation and migration of HCC cells, and stimulate the expression of PD-L1 through activating the PI3K/Akt signaling pathway in HCC cells.

Conclusions: PKM2 was able to upregulate the expression of PD-L1 and stimulate the malignant behaviors of HCC cells. Targeting PKM2 is a promising strategy for liver cancer treatment.

Key words: pyruvate kinase M2, hepatocellular carcinoma, Warburg effect, PD-L1, malignant behaviors, PI3K/Akt signaling pathway.

Introduction

Hepatocellular carcinoma (HCC) is a global health challenge, and its incidence is expected to exceed 1 million by 2025. HCC is the most com-

mon type of liver cancer, and hepatitis B and C virus infections are the major risk factors for HCC development [1, 2]. Hepatectomy, liver transplantation, ablative therapy, and transcatheter chemoembolization are the main treatment methods for early- and middle-stage liver cancers. Systematic treatment is recommended for patients with advanced liver cancer. Sorafenib and lenvatinib have been used as first-line treatments for advanced liver cancer for more than 10 years. However, the response rate to these tyrosine kinase inhibitors (TKI) is low, and adverse events often occur during systemic therapy in advanced HCC patients [3]. In recent years, immune checkpoint inhibitors (ICIs) have become a primary therapeutic approach for advanced HCC. ICIs prevent T-cell inactivation by blocking the interaction between checkpoint proteins and their ligands. For example, inhibitors of programmed cell death protein 1 (PD-1)/ligand 1 (PD-L1) have been used [4].

PD-1 is one of the key co-suppressor receptors expressed on T cells during T cell activation and plays an important role in suppressing the immune response by regulating T cell activity, activating apoptosis of antigenic T cells, and inhibiting apoptosis of regulatory T cells (Tregs) [5]. PD-L1 is a transmembrane glycoprotein that is overexpressed on the surface of malignant tumor cells [6]. In the HCC tumor microenvironment, PD-L1 is mainly expressed in Kupffer cells but is less expressed in other antigen-presenting cells (APC) or HCC cells. Moreover, the increased expression of PD-L1 in liver cancer is positively correlated with poor prognosis in patients with liver cancer and shorter overall survival [7]. The activation of PD-1 can significantly inhibit T cell receptor (TCR), CD28 co-stimulator, and inducible T cell co-stimulator (ICOS) signaling, effectively inhibiting T cell activation. Thus, tumor cells evade immune surveillance [8].

Glucose metabolism is a complex process, and there is considerable evidence that dysregulation of glucose metabolism is a recognized focus in the development and progression of HCC [9–11]. Normal cells decompose glucose into lactic acid under anaerobic or hypoxic conditions and simultaneously produce a small amount of ATP at the same time. However, owing to the energy demand for rapid proliferation, tumor cells also undergo glycolysis under aerobic conditions to rapidly produce ATP, which is called aerobic glycolysis or the Warburg effect [12]. As glucose metabolism in tumor cells and lactic acid secretion increases, the pH value in the tumor microenvironment (TME) decreases, and acidosis has multiple effects on tumor cells [13]. On one hand, acidosis promotes local invasive growth and metastasis of tumor cells, and the region with the highest tumor invasion corresponds to the region with the lowest pH value [14, 15]. The glucose consumption of tumors restricts the metabolism of T cells, and nutrient competition between tumor cells and T cells affects the activity and function of T cells and mediates their low reactivity of T cells [16].

Pyruvate kinase (PK) is a key enzyme in glycolysis that converts phosphoenolpyruvate (PEP) to pyruvate. Pyruvate kinase M2 (PKM2), an isoform of PK, plays an important role in the occurrence and development of tumors [17, 18]. Several studies have shown that PKM2 is significantly upregulated in breast [19], pancreatic [20], bladder [21], HCC [22], and other cancers. PKM2 exists in both dimeric and tetrameric forms and is allosterically regulated by exogenous activators and inhibitors. When PKM2 is in the tetramer state, it has a higher affinity for the substrate PEP and higher enzyme activity, while PKM2 can enter the nucleus as a transcription factor to activate the transcription of certain genes. It can also regulate other proteins in the cytoplasm [23, 24] and activate the enzymatic activity of cytoplasmic proteins.

The PI3K/Akt/mTOR signaling pathway is abnormally activated in many tumorigenesis processes and plays a key role in tumorigenesis and development by participating in the cell cycle and promoting angiogenesis, tumor invasion, and metastasis [25]. The PI3K/Akt/mTOR signaling pathway can also regulate the expression of PD-L1 [26–28]. The use of PI3K/Akt/mTOR related inhibitors will reduce the expression of PD-L1, while the stimulation of PI3K/Akt can increase the expression of PD-L1 [29]. In glioma cells with PTEN deletion, Akt is activated and PD-L1 is significantly expressed after Akt activation. After treating cells with phosphoinositol analogs to block Akt activation, the expression of PD-L1 is decreased, and after transfecting cells with viruses to restore PTEN function, the expression of PD-L1 is also decreased [30, 31]. Interferon γ (IFN-γ) is the most important cytokine in anti-tumor immunity and IFN-γ induces PD-L1 expression in tumor cells. Treatment of lung cancer cells with the PI3K inhibitor Ly294002 leads to the downregulation of IFN-γ-induced PD-L1 mRNA expression [32]. Since the PI3K/Akt/mTOR signaling pathway is closely related to glucose metabolism in tumor cells and regulates the expression of PD-L1 to a certain extent [33], we speculated that there is a relationship between glucose metabolism reprogramming (Warburg effect), PI3K/Akt/mTOR, and PD-L1. This study aimed to explore the influence of PKM2 on PD-L1 expression and malignant behaviors in HCC cells and its regulatory mechanisms through biological information databases, clinical tissue, and cellular molecular levels. Additionally, the study explored how lactic acid, a product of the Warburg effect, influences the expression of PD-L1 and malignant behavior of liver cancer cells, in order to provide new insights for liver cancer immunotherapy.

Material and methods

Collection and analysis of clinical patient samples

Thirty patients with a clinical or pathological diagnosis of liver cancer admitted to the Second Affiliated Hospital of Hainan Medical University between January 2021 and December 2022 were enrolled. The exclusion criteria were as follows: active bleeding within the last 6 months; patients with a history of blood transfusion within the past 1 month; and patients who had an acute infection or inflammatory reaction within the last 3 months. All subjects provided written informed consent, and the collection and use of tissue specimens were approved by the Medical Ethics Committee of the Second Affiliated Hospital of Hainan Medical University. Ethical board approval (number Med-Eth-Re[2022]279) and informed consent were obtained from all participants, and the expression of target proteins was detected in the samples (Medical Ethics Statement: This project collected more than 30 cases of normal liver tissues, blood cells, other normal tissues and liver cancer tissues; the tissues were used for analysis by immunochemistry, Western blotting, fluorescence chemistry and other techniques to detect the expression of PD-L1, PKM2 and HK2 in these tissues, and to determine the highly specific expression of PD-L1, PKM2 and HK2 in liver cancer cells. We believe that the above information is true and that this study complies with the principles of the Declaration of Helsinki and the relevant laws and regulations of our country. We promise to abide by medical ethics, academic norms, consciously fulfill relevant obligations, and fully respect the rights and interests of research subjects).

Cell culture

In this study, the human HCC cell lines Bel7402 and Huh7 were selected. Bel7402 cells were purchased from Bode Biological Company, and Huh7 cells were obtained from the Joint Laboratory of Tropical Infectious Diseases of Hainan Medical University and the Hong Kong University. Short tandem repeat (STR) identification was performed in Bel7402 and Huh7 cell lines. Frozen Bel7402 and Huh7 cells were placed in a water bath at 37°C. After the frozen solution was thawed, it was resuscitated in a sterile laminar flow hood sterilized by ultraviolet light. DMEM containing 10% fetal bovine serum was used for the cell culture. Medium (5 ml) was added to each cell culture bottle. It was then placed in a 5% CO_2 incubator at 37°C. After 24 h, the cells were observed under a microscope, and the culture medium was replaced.

Bioinformatics analysis

The Gene Expression Omnibus (GEO) database of Clinical Health Trust Home (http://www.aclbi.com) includes all tumor types, integrated dataset screening (in Chinese and English), keyword screening for sample information, one-click probe ID conversion, batch effect removal, and data standardization. Analyses, including differential genes, gene correlations, and immune checkpoints, were performed. The TCGA database was used to analyze the relevance of genes (http://cancergenome.nih.gov), the RNA-seq data of PKM2 and CD274 were downloaded from The Cancer Genome Atlas (TCGA) database, and the molecular correlation analysis of PKM2 and CD274 was performed using R language (version 3.6.3). The R package ggplot (version 3.3.3) was used for analysis. The Search Tool for the Retrieval of Interacting Genes/Proteins (STRING) database (http://cn.string-db.org/) provides a pathway in which the target protein may participate. (1) Protein Name: Enter the protein name and click on the search. (2) Select Homo sapiens and click continuously; (3) Proteins that can interact with PD-L1 can appear; (4) After the desired protein interaction interface appears, click on Analysis→Kyoto Encyclopedia of Genes and Genomes (KEGG) Pathways to query the signaling pathways that PD-L1 may participate in.

Immunohistochemistry

First, the excised liver cancer tissues and paired para-cancerous tissues were fixed with 4% paraformaldehyde for more than 24 h, and then dehydrated in a dehydrator according to a certain concentration of ethanol. The dehydrated tissues were then embedded. According to the specific requirements of the tissue chip matrix, the removed tissue points were placed into the corresponding wax block holes in sequence, the tissue points were fused with the wax block with the tissue chip fusion instrument, and then the tissue chip was placed in the microtome to cut approximately 4 μm of slices. The sections were then stained with hematoxylin-eosin (HE), and the staining results were observed under a microscope. The sections also needed to be dewaxed, soaked in water, repaired by antigen, blocked with hydrogen peroxide, incubated at 4°C for the first antibody overnight, and incubated at room temperature with the second antibody for 1 h. DAB color developing solution was added for DAB color development. Cell nuclei were re-stained with hematoxylin, dehydrated, sealed, observed under a microscope, and analyzed with Aipathwell software.

Lentivirus transfection and screening of stable expression cell lines

The number of Bel7402 cells and Huh7 cells in the logarithmic growth stage was adjusted to 1.5 × 10^5 cells/ml, which were spread on 24-well plates at 500 /well and incubated in a 5% CO_2 incubator at 37°C for 24 h. On the second day, the 24-well plate culture medium was discarded, and 250 µl of fresh culture medium containing infection booster solution 1×HitansG A or 1×HitansG P was added to each well. The corresponding viral volume was converted according to the selected multiplicity of infection (MOI) gradient, and the virus was added to the culture medium. Cells transfected with the virus were cultured in an incubator for 4 h, after which 250 µl of fresh medium (without infection-enhancing fluid) was added. The culture was continued for approximately 15 h, the original culture medium was discarded, and the fresh medium was replaced. Infection efficiency was examined under a fluorescence microscope after 48 and 72 h. Before screening stable strains, the minimum concentration of purinomycin to kill cells in the blank group was explored in advance, and the cells in the blank group were spread on 24-well plates to ensure that the fusion rate of cells reached approximately 80% on the second day. After 24 h, the cells were replaced with fresh medium containing purinomycin, and the concentration gradient of purinomycin was set as follows: 0, 0.5, 1, 1.5, 2, 2.5 µg/ml. The minimum concentration that could completely kill cells in 5 days was selected as the screening concentration for follow-up experiments. After 72 h of lentivirus infection, the stable P1 cell line was obtained by screening with the discovered concentration of purinomycin, the concentration of which was reduced to 50% of the original concentration. The cell line was cultured with half of the concentration of purinomycin to maintain the resistance of the cells.

Immunofluorescence

Cells with good growth status were selected, and the number of cells was adjusted to 3 × 10^4/ml. A 300 µl cell suspension was placed at the bottom of a glass substrate petri dish and cultured in an incubator for 24 h until the cells were attached to the wall. The cells were then fixed with 4% paraformaldehyde for 30 min. After fixation, quick block immunostaining blocking solution was added for sealing and permeability. The primary antibody was diluted to 1 : 100 and incubated overnight at 4°C. The secondary antibody Alexa Fluor 647 with fluorescent labeling was incubated at room temperature in the dark for 1 h the next day. 4′,6-diamidino-2-phenylindole (DAPI) staining solution was added for nucleation for 30 min, and an anti-fluorescence quencher was added to seal the film and observed under a laser confocal microscope.

Cell scratch test

A marker pen was used to mark the three horizontal lines evenly with a ruler behind the 6-well plate, and an appropriate number of cells was added to the 6-well plate. The inoculation principle was that the fusion rate could reach 100% after an overnight incubation. The next day, when the cells were overgrown, scratches were made with the gun head perpendicular to the cell plane, washed three times with PBS, and then the fresh medium was replaced. The cells were cultured in an incubator and removed at appropriate time points (0, 24, 48, 72 h). The degree of healing was observed under an inverted microscope and photographs were taken.

Plate cloning experiment

Cells with good growth status were selected and inoculated into 6-well plates at approximately 500 cells/well and cultured in incubators. After 2 weeks, the 6-well plate was removed, the culture medium was removed, the plate was fully cleaned with PBS, and 1 ml of 4% paraformaldehyde was added to each well and fixed for 30 min. After cleaning with PBS twice, 0.1% crystal violet was added and the cells were stained for 30 min. The 6-well plate was then rinsed with running water, air-dried, and subjected to colony counting and photography.

Transwell migration experiment

After centrifugation of the well-grown cells, the cell precipitate was diluted to 5 × 10^5/ml with serum-free medium, and 500 µl of 20% FBS medium was added to the lower chamber of a 24-well plate. The sterile Transwell chamber was placed into the well, 200 µl of the cell suspension was added into the Transwell chamber, and the culture was continued for 48 h in the incubator. The cells were then removed, washed twice with PBS, and fixed in 4% paraformaldehyde for 20 min. After fixation, the cells were placed in 0.1% crystal violet staining solution for 20 min and the number of cells passing through the cells was observed under an inverted microscope.

EdU cell proliferation test and reagent kit were applied to detect the contents of lactic acid, pyruvate, ATP and consumption of glucose

The EdU (5-ethynyl-2′-deoxyuridine) cell proliferation assay was performed using an EdU-555 cell proliferation assay kit (Shanghai Beyotime Biotech Co., Ltd.). The lactic acid content was detected using lactic acid assay kit (Nanjing Jiangjian Co., Ltd.). The pyruvate content was determined

using a pyruvate acid assay kit (Beijing Sarlobio Life Science Technology Co., Ltd.). ATP content was detected using an enhanced ATP detection kit (Shanghai Beyotime Biotech Co., Ltd.), and glucose content was detected using a glucose detection kit (Beijing Sarlobio Life Science Technology Co., Ltd.).

Protein immunoblotting

The cell precipitate was collected by centrifugation, and the total protein of the cells was extracted according to the instructions of the Total Protein Extraction Kit (Shanghai Sangon Biotech Co., Ltd.). The protein concentration of each sample was measured using an enhanced BCA protein concentration kit (Shanghai Beyotime Biological Technology Co., Ltd.). SDS-PAGE was performed using 10% separation gel and 5% spacer gel. After electrophoresis, the gel with the corresponding bands was cut off, and the membrane was transferred to a 0.45 μm PVDF membrane. The PVDF membranes were incubated in a sealing solution (Shanghai Yase Biomedical Technology Co., Ltd.) at 37°C for 15 min. The dilution ratio of hexokinase 2 (HK2) and hypoxia-inducible factor 1α (HIF-1α) to the primary antibody was 1 : 2000, and the dilution ratio of other primary antibodies was 1 : 1000. The PVDF membrane was placed with primary antibody and incubated at 4°C for 16 h. The PVDF membrane was placed into the diluted secondary antibody, incubated at 37°C for 1 h, and finally developed and photographed. All the antibodies were purchased from Abcam, Proteintech Group, and Affinity Biosciences.

Statistical analysis

The experiment was repeated at least three times in each group. ImageJ image software was used to analyze the strip gray value and scratch area, and the cell counts were determined. Experimental data are presented as the mean standard ± deviation ($\bar{x} \pm s$), and statistical analysis was performed using GraphPad Prism software (version 9.0). The *t*-test or χ^2 test was used for analysis between two groups, ANOVA was used for comparison among multiple groups, and Pearson or Spearman correlation analysis was used for correlation analysis of the two variables. $P < 0.05$ was considered statistically significant.

Results

Expression and correlation analysis of PKM2 and PD-L1 in biological information database

To understand the correlation between PKM2 and PD-L1 in liver cancer tissues, 144 samples (72 liver cancer specimens and 72 normal tissues) in the GEO (https://www.ncbi.nlm.nih.gov/geo/) database of clinical Bioinfo Home were first analyzed, and it was found that the expression level of PKM2 in liver cancer tissues was significantly higher than that in normal tissues ($p < 0.0001$), as shown in Figure 1 A. The TCGA (/ccg/research/genome-sequencing/tcga) database was used to analyze the correlation between PKM2 and PD-L1 in liver cancer tissues, and it was found that the expression level of PKM2 was positively correlated with PD-L1 ($p < 0.001$), as shown in Figure 1 B. Finally, the Analysis-KEGG (https:// www.genome.jp/kegg/) Pathway was analyed using the STRING database revealed that PD-L1 may be related to the PI3K/Akt signaling pathway ($p < 0.001$), as shown in Figure 1 C.

Western blotting detected the expression of PKM2 and PD-L1 in liver cancer tissues and paired para-cancerous tissues

To explore the expression of PKM2 and PD-L1 in liver cancer, tissue samples from 30 patients with liver cancer were analyzed, with T representing liver cancer tissue and P representing the paired para-cancerous tissues. The results of Western blotting experiments showed that the expression levels of PKM2 and PD-L1 in cancer tissues were significantly higher than those in the paired para-cancerous tissues. The gray values of the bands were analyzed using ImageJ software, and the difference was statistically significant ($p < 0.05$), whereas the expression of HK2 in cancer tissues and paired para-cancerous tissues was not statistically significant (Figures 2 A, B).

The expression of PD-L1, PKM2, and HK2 in liver cancer tissues and paired para-cancerous tissues was detected by immunohistochemistry

Cancerous tissues and paired para-cancerous tissues of 30 HCC patients were prepared into tissue chips, with T representing liver cancer tissue and P representing the paired para-cancerous tissues, as shown in Figure 3 A. The expression of PD-L1, PKM2, and HK2 was detected by immunohistochemistry, and the density of positive cells in the sections was analyzed using the Aipathwell software. The results showed that the density of positive cells of PD-L1 in liver cancer tissues was higher than that in paired para-cancerous tissues (Figures 3 B, C) ($p < 0.05$). The expression of PKM2 in liver cancer tissues was significantly higher than that in paired para-cancerous tissues, as shown in Figures 3 B and D. PKM2 expression in liver cancer tissues was positively correlated with the expression of PD-L1, which was consistent with the re-

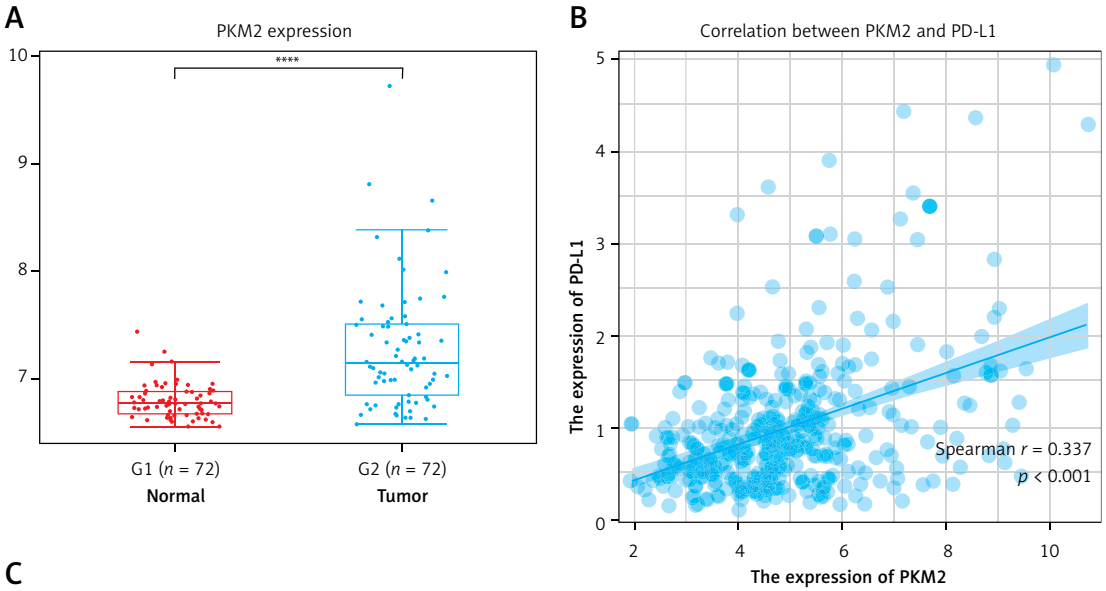

C

ONTOLOGY	ID	Description	GeneRatio	pvalue	p.adjust
KEGG	hsa05235	PD-L1 expression and PD-1 checkpoint pathw	14/36	0.000000000000	0.000000000000
KEGG	hsa04660	T cell receptor signaling pathway	12/36	0.000000000000	0.000000000001
KEGG	hsa04658	Th1 and Th2 cell differentiation	11/36	0.000000000000	0.000000000005
KEGG	hsa04659	Th17 cell differentiation	11/36	0.000000000001	0.000000000021
KEGG	hsa04514	Cell adhesion molecules	12/36	0.000000000001	0.000000000024
KEGG	hsa04151	PI3K-Akt signaling pathway	9/36	0.000017747525	0.000103989222
KEGG	hsa04672	Intestinal immune network for IgA productior	7/36	0.000000001417	0.000000028941
KEGG	hsa01521	EGFR tyrosine kinase inhibitor resistance	8/36	0.000000001417	0.000000028941
KEGG	hsa05320	Autoimmune thyroid disease	7/36	0.000000002510	0.000000044866
KEGG	hsa05330	Allograft rejection	6/36	0.000000012622	0.000000200554
KEGG	hsa05332	Graft-versus-host disease	6/36	0.000000023680	0.000000338623
KEGG	hsa04940	Type I diabetes mellitus	6/36	0.000000027432	0.000000356618
KEGG	hsa04014	Ras signaling pathway	10/36	0.000000041624	0.000000496023
KEGG	hsa05323	Rheumatoid arthritis	7/36	0.000000135935	0.000001495289
KEGG	hsa04640	Hematopoietic cell lineage	7/36	0.000000209592	0.000002033974
KEGG	hsa05416	Viral myocarditis	6/36	0.000000213354	0.000002033974
KEGG	hsa05166	Human T-cell leukemia virus 1 infection	9/36	0.000000335070	0.000002994686
KEGG	hsa05340	Primary immunodeficiency	5/36	0.000000595343	0.000005007886
KEGG	hsa04722	Neurotrophin signaling pathway	7/36	0.000000740235	0.000005880754
KEGG	hsa04650	Natural killer cell mediated cytotoxicity	7/36	0.000001419669	0.000010684881

Figure 1. The expression and correlation of PD-L1 and PKM2 in liver cancer tissues were analyzed using bioinformatics databases. **A** – Expression of PKM2 in liver cancer tissues and normal tissues in GEO database, $p < 0.0001$. **B** – The correlation between PD-L1 and PKM2 in liver cancer tissues was analyzed using the TCGA database, $p < 0.001$. **C** – KEGG pathway analysis in String database, PD-L1 related molecules and signaling pathways, $p < 0.001$

sults of bioinformatics analysis, and the difference was statistically significant ($p < 0.05$), as shown in Figure 3 E. In addition, the expression of HK2 in liver cancer tissues was significantly higher than that in paired para-cancerous tissues ($p < 0.05$) (Figure 3 F).

Stable PKM2-silenced and PKM2-overexpressing cell lines were successfully established

In the present study, we used Western blotting to detect the expression of PKM2 in the HCC cell lines Huh7 and Bel7402. The results indicated that Bel7402 highly expressed PKM2, Huh7 expressed low levels of PKM2, and the expression of PKM2 in Bel7402 cells was significantly higher than that in Huh7 cells (Figure 4 A). To explore the influence of PKM2 in glucose metabolic reprogramming, Bel7402 and Huh7 cells were selected for lentiviral (LV) transfection with short hairpin(sh) RNA to interfere with PKM2-expressed vectors or PKM2-overexpressed vectors, respectively. LV-shPKM2 lentivirus or short hairpin(sh) negative control (shNC) lentivirus was used to infect the Bel7402 cell line (with relatively high PKM2 expression), and the cell transfection rate was

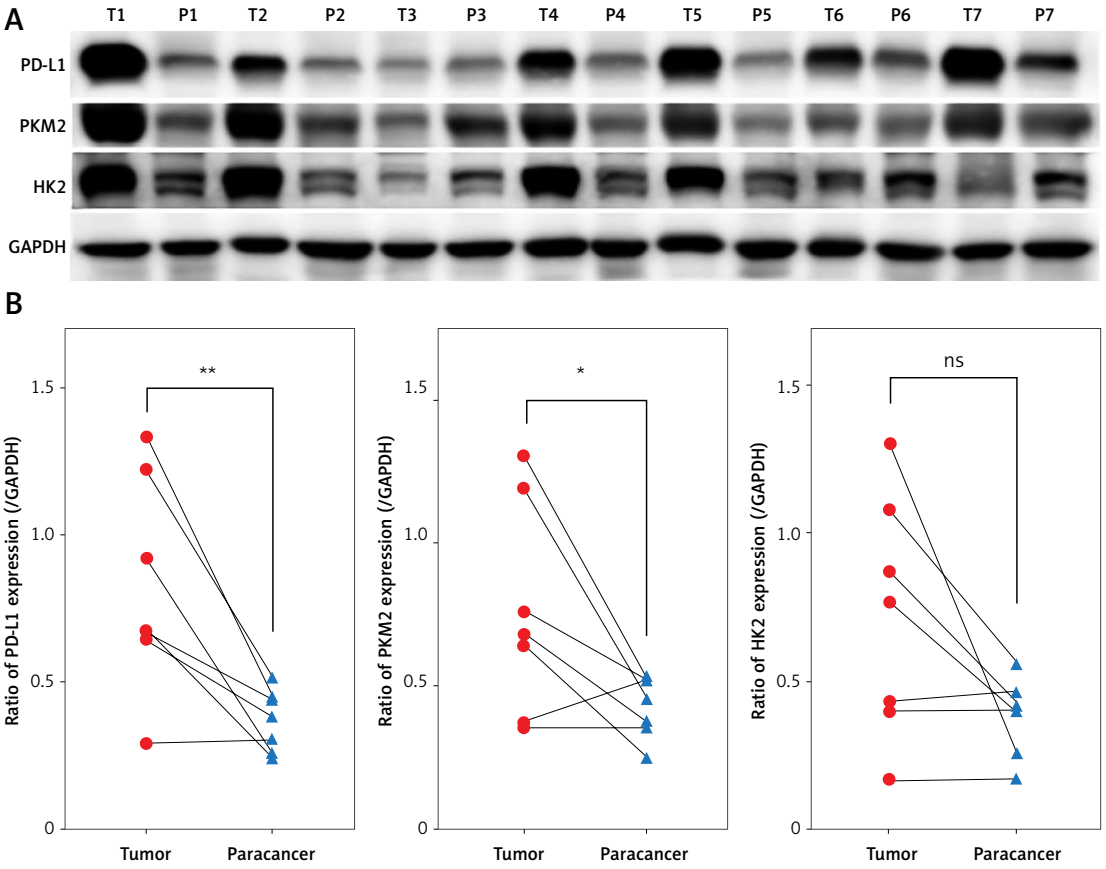

Figure 2. Western blotting results showed the expression of PD-L1, PKM2, and HK2 in cancerous tissues and paired para-cancerous tissues. T is the liver cancer tissues, P is the paired para-cancerous tissues, the protein sample size per pore is 20–50 μg, the bottom chart is the statistical map of each group after gray scale analysis, $^{**}p < 0.01$, $^{*}p < 0.05$. Data are shown as mean ± SD ($n = 14$). *P*-values were calculated using the unpaired two-sided Student's *t* test

observed under an inverted fluorescence microscope after infection with LV for 72 h, as shown in Figure 4 B. Green fluorescent cells accounted for more than 90%, and purinomycin was used for screening. Seven days later, the expression of PKM2 was detected by Western blotting. The expression of PKM2 protein in the shPKM2 vector-transfected group (Bel7402-shPKM2) was significantly lower than that in the negative control (NC) vector-transfected group (Bel7402-shNC) and the control group (Bel7402) ($p < 0.01$), as shown in Figure 4 C. These results indicated that the Bel7402-shPKM2 cell line was successfully constructed to silence the expression of PKM2. To establish cell lines overexpressing PKM2, Huh7 cells (PKM2 had relatively low expression) were infected with PKM2-expressed lentivirus (LV-PKM2) or lentivirus negative control (LV-NC), and the cell transfection rate was observed under an inverted fluorescence microscope after transfection with LV for 72 h. Green fluorescent cells accounted for more than 90% of the cells, as shown in Figure 4 D. Seven days later, the expression of PKM2 was detected using Western blotting. As shown in Figure 4 E, the expression of PKM2 protein in the LV-PKM2 vector group (Huh7-PKM2) was significantly higher than that in the lentivirus negative control group (Huh7-NC) and the control group (Huh7) ($p < 0.01$). These results indicated that Huh7-PKM2 cell lines overexpressing PKM2 were successfully constructed.

The localization of PD-L1 in Bel 7402 and Huh7 cells was observed using laser confocal microscopy. As shown in Figures 4 F and 4 G, blue DAPI is the nucleus and red is the marked PD-L1. After the fusion of the two colors, it can be seen that PD-L1 was mainly located in the cytoplasm and cell membrane, and the expression level in the nucleus was low. Moreover, the red brightness of the shPKM2 vector-transfected group (Bel7402-shPKM2) was significantly lower than that of the negative control vector group (Bel7402-shNC) and control group (Bel7402) (Figure 4 F), suggesting that silencing the expression of PKM2 may reduce the expression of PD-L1. However, in Huh7 cells, the red brightness in the LV-PKM2 vector-transfected group (Huh7-PKM2) was significantly higher than that in the negative control vector-transfected group (Huh7-NC) and the control group (Huh7) (Figure 4 G), suggesting that overexpression of

A

Marker									
T1	P1	T7	P7	T13	P13	T19	P19	T25	P25
T2	P2	T8	P8	T14	P14	T20	P20	T26	P26
T3	P3	T9	P9	T15	P15	T21	P21	T27	P27
T4	P4	T10	P10	T16	P16	T22	P22	T28	P28
T5	P5	T11	P11	T17	P17	T23	P23	T29	P29
T6	P6	T12	P12	T18	P18	T24	P24	T30	P30

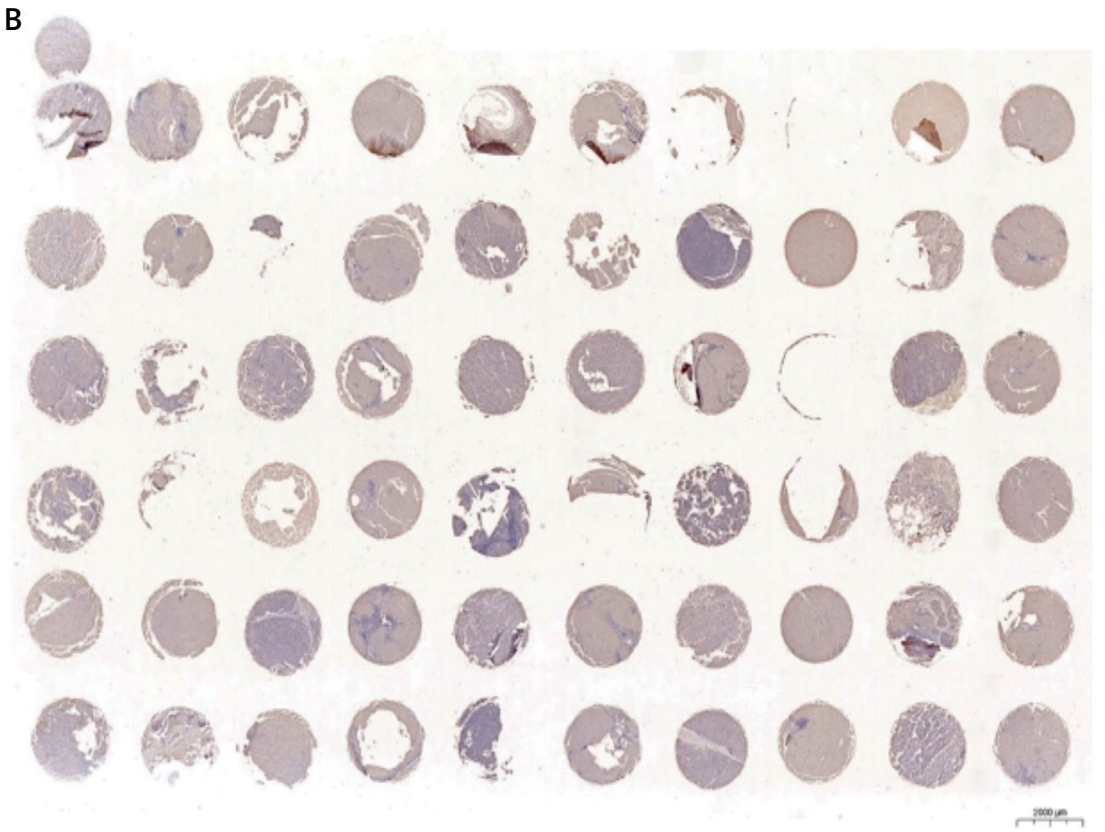

Figure 3. Immunohistochemical analysis of PD-L1, PKM2, and HK2 expression in cancerous tissues and corresponding para-cancerous tissues. **A** – Histochip matrix of 30 cases of cancer tissues and paired para-cancerous tissues, where T is cancerous tissues and P is paired para-cancerous tissues. **B**, **C** – Expression of PD-L1 in HCC tissues was detected by immunohistochemistry. The PD-L1 staining intensity of cancer tissue is strongly positive, while the PD-L1 staining intensity of para-cancerous tissues is weakly positive. Imaged at magnification 40× (scale bar: 20 μm). Positive cell density = number of positive cells/tissue area to be measured. The chart on the right is the statistical graph after analysis of PD-L1 positive cell density in sections by Aipathwell software, $*p < 0.05$

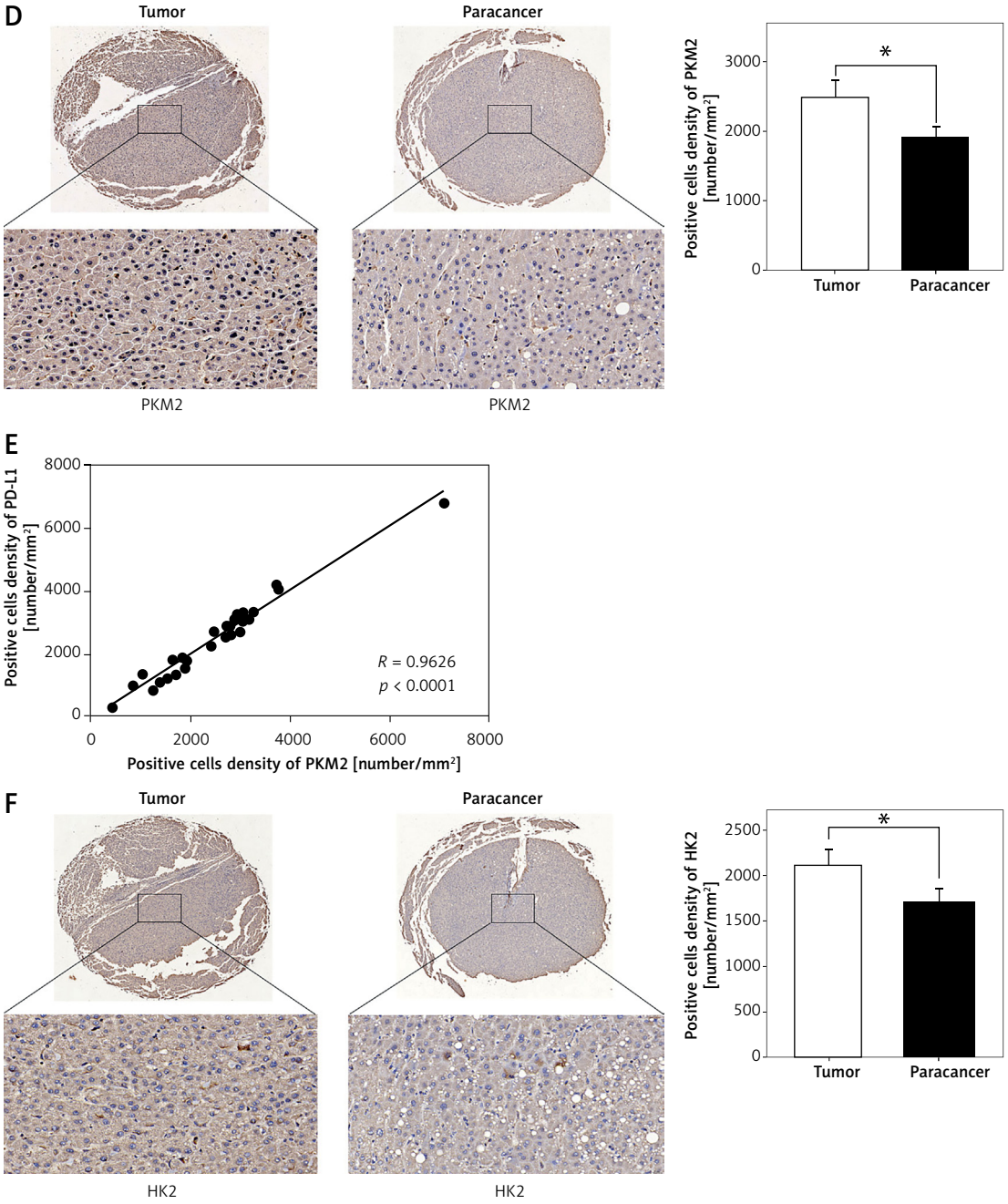

Figure 3. Cont. **D** – The expression of PKM2 in HCC tissues was detected by immunohistochemistry. The PKM2 staining intensity of cancer tissue is moderately positive, while the PKM2 staining intensity of para-cancerous tissues is weakly positive. Imaged at magnification 40× (scale bar: 20 μm). Density of positive cells = number of positive cells/area of tissue to be measured. The charts on the right are the statistical charts after analysis of the density of positive PKM2 cells in the sections by Aipathwell software. **E** – Correlation analysis diagram of PD-L1 and PKM2 in 30 liver cancer tissues, $^*p < 0.05$. **F** – Immunohistochemistry was performed to detect the expression of HK2 in HCC tissues of HCC patients. The HK2 staining intensity of cancer tissue is moderately positive, while the HK2 staining intensity of para-cancerous tissues is weakly positive. Imaged at magnification 40× (scale bar 20 μm). Density of positive cells = number of positive cells/area of tissue to be measured. The chart on the right shows the statistical graph of HK2 positive cell density in sections analyzed by Aipathwell software, $^*p < 0.05$. Data are shown as mean ± SD ($n = 60$). *P*-values were calculated using unpaired two-sided Student's *t* test

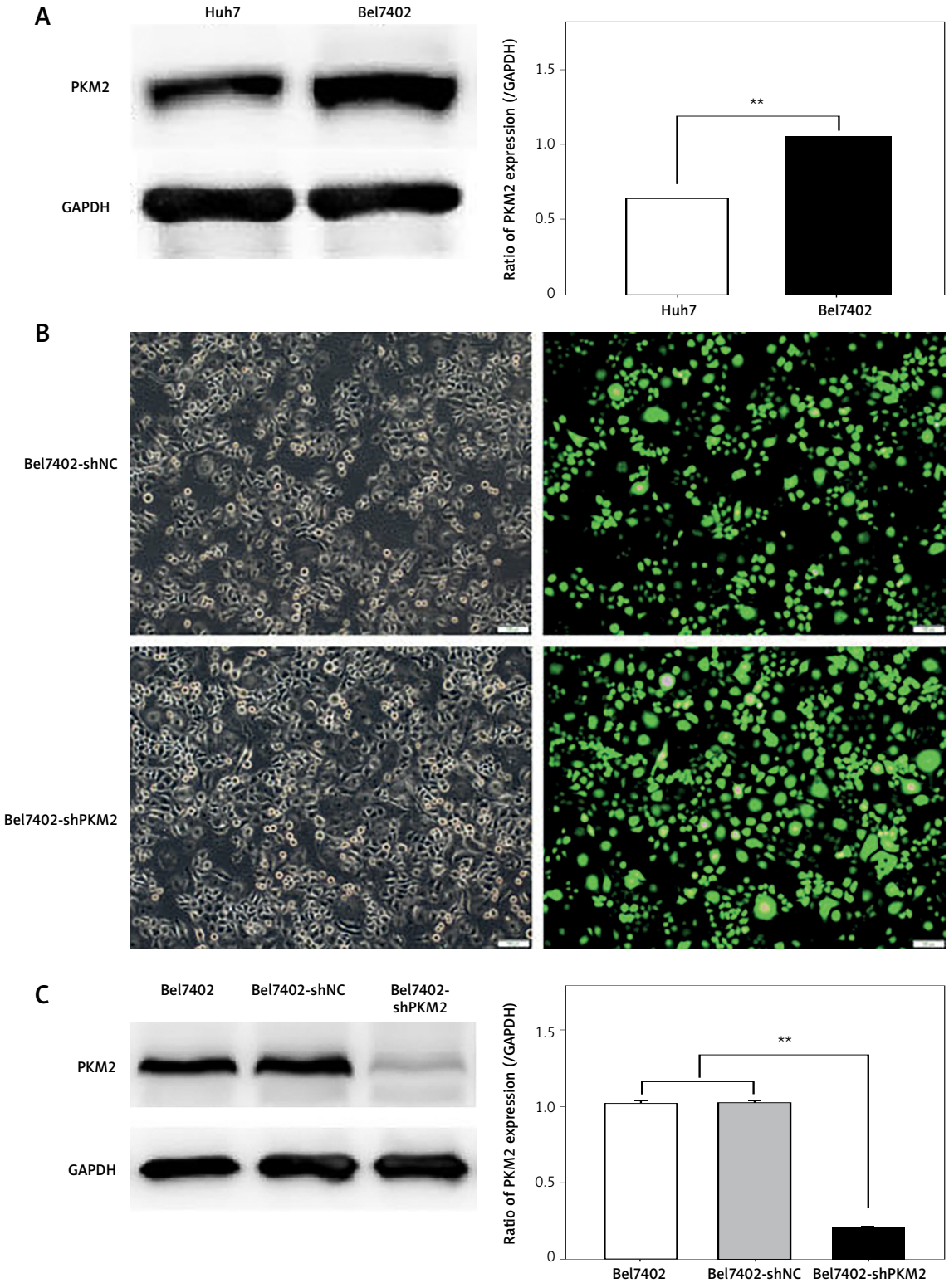

Figure 4. Establishment of stable PKM2-silenced and PKM2-overexpressing cell lines. **A** – Western blotting detected the expression of PKM2 protein in Bel7402 and Huh7 cells, and the protein sample size per well was 20–50 µg. The chart on the right is the statistical map of PKM2 bands after gray scale analysis, $^{**}p < 0.01$. **B** – Fluorescence expression of LV-shPKM2 infected Bel7402 cells. Fluorescence images were taken with a 10× objective lens with a scale bar of 100 µm. **C** – Western blotting detected the expression of PKM2 in Bel7402-shPKM2 cells, and the protein sample size per well was 20–50 µg. The chart on the right is the statistical map of PKM2 bands after gray scale analysis, $^{**}p < 0.01$

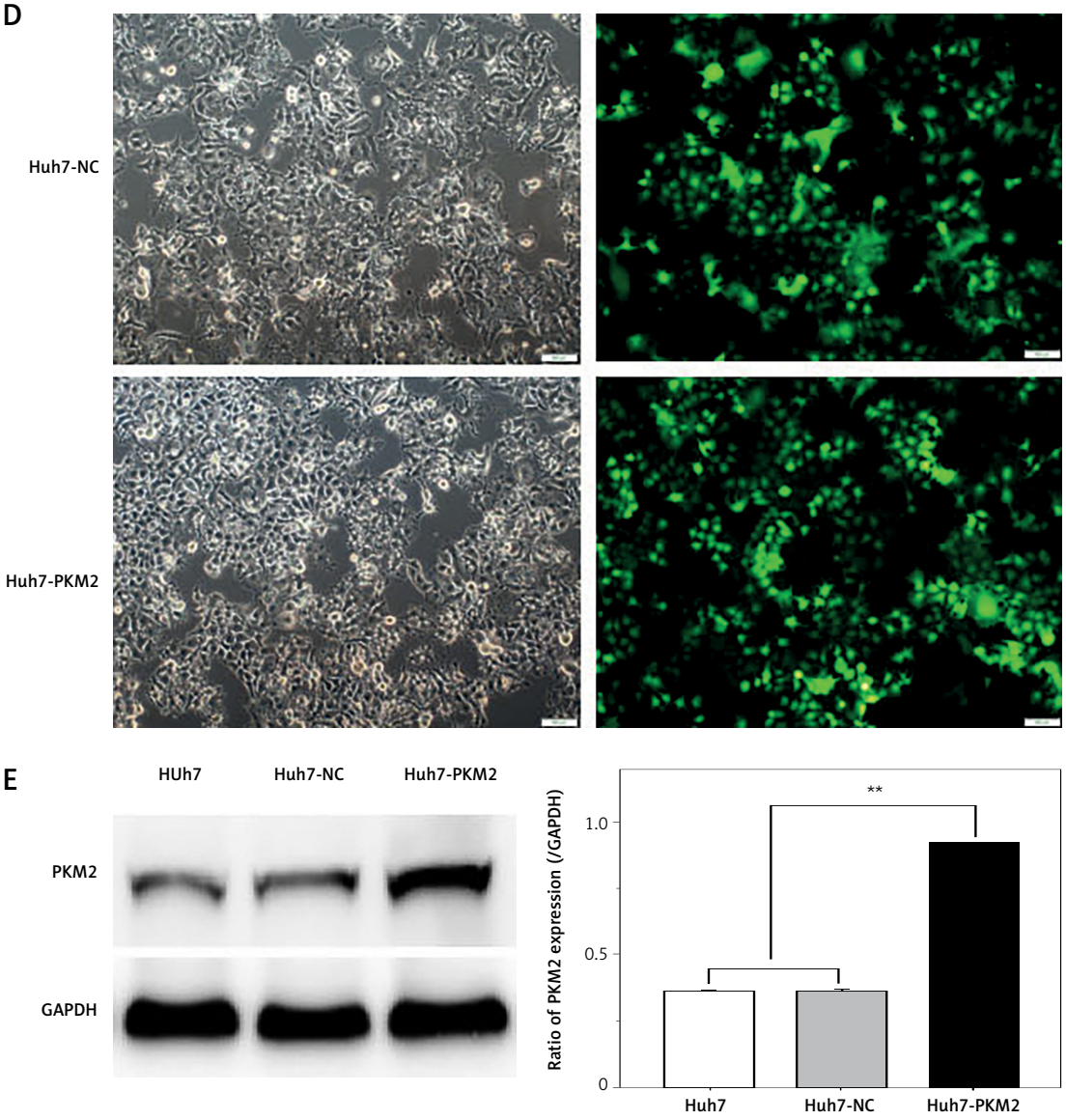

Figure 4. Cont. **D** – Fluorescence expression of LV-PKM2 infected Huh7 cells. Fluorescence images were taken with a 10× objective lens and the scale was 100 µm. **E** – Western blotting was used to detect the expression of PKM2 in Huh7-PKM2 cells, and the protein sample size per pore was 20–50 µg. The chart on the right was the statistical map of PKM2 bands after gray scale analysis, $^{**}p < 0.01$

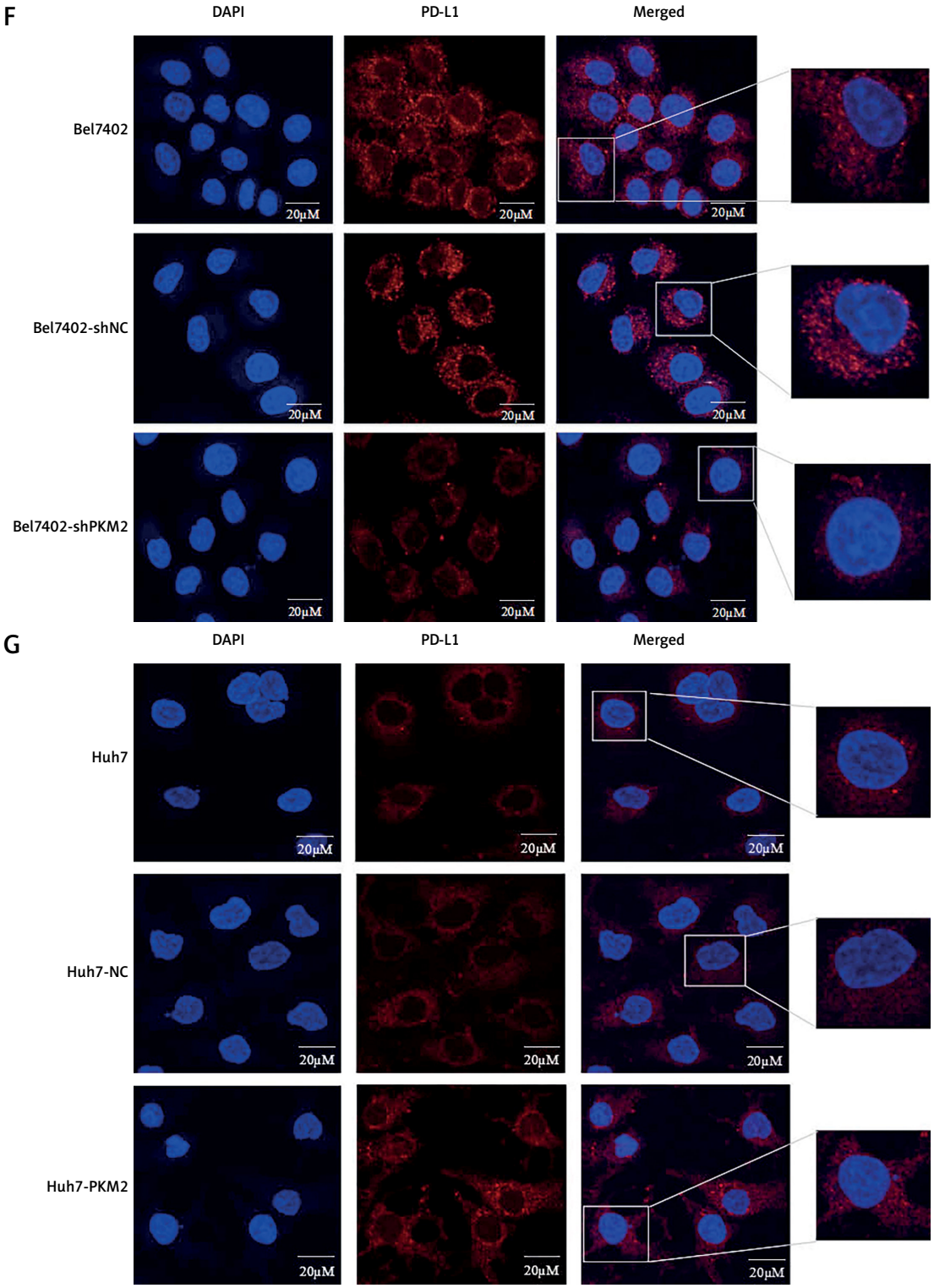

Figure 4. Cont. **F** – Expression and localization of PD-L1 in Bel7402 were observed by laser confocal microscopy. **G** – Expression and localization of PD-L1 in Huh7 cells were observed by laser confocal microscopy. Data are shown as mean ± SD from three independent experiments (n = 3). Statistical differences were determined with one-way ANOVA

PKM2 may increase the expression level of PD-L1 in HCC cells. These results indicated that stability silencing the expression of PKM2 and stable overexpression of PKM2 was successfully established, and that PKM2 was able to stimulate the expression of PD-L1 in HCC cells.

PKM2 stimulates malignant behaviors of HCC cells

The pivotal factors of poor prognosis in liver cancer are mainly intrahepatic metastasis and distant metastasis, and the basic factor of cancer cell metastasis is the increase in cell metastatic ability; however, whether PKM2 affects the metastatic ability is still unclear. Cell scratch experiments revealed that the healing ability of Bel7402 cells (Bel7402-shPKM2) silenced with PKM2 was significantly reduced, whereas that of Huh7 cells (Huh7-PKM2) overexpressing PKM2 was significantly enhanced. These results suggested that PKM2 knockdown may weaken the healing and repair abilities of HCC cells, and overexpression of PKM2 may enhance the healing and repair abilities of HCC cells. The scratch area was analyzed using ImageJ software, and the healing and repair rates were statistically analyzed, showing statistically significant differences ($p < 0.01$), as shown

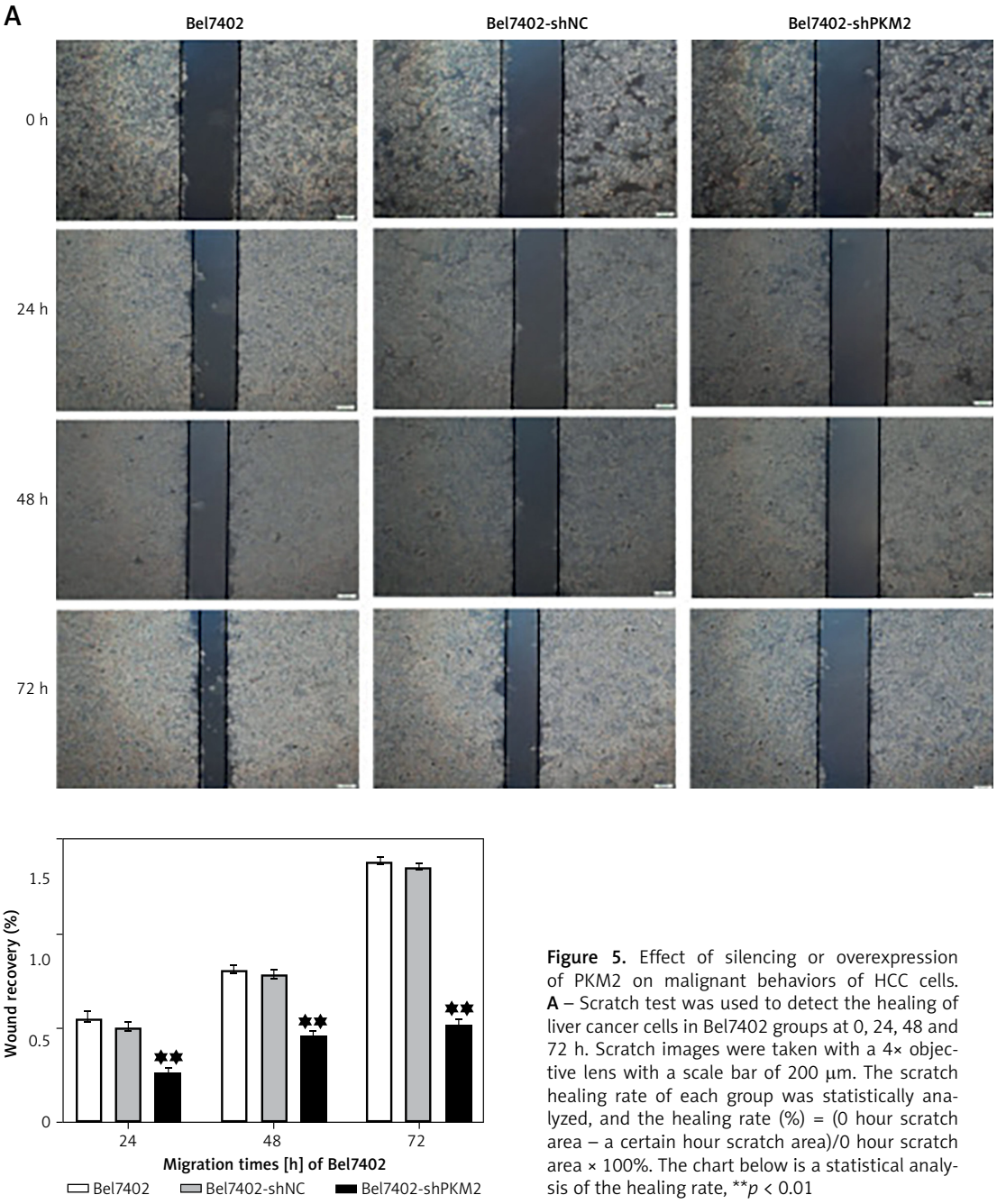

Figure 5. Effect of silencing or overexpression of PKM2 on malignant behaviors of HCC cells. **A** – Scratch test was used to detect the healing of liver cancer cells in Bel7402 groups at 0, 24, 48 and 72 h. Scratch images were taken with a 4× objective lens with a scale bar of 200 μm. The scratch healing rate of each group was statistically analyzed, and the healing rate (%) = (0 hour scratch area – a certain hour scratch area)/0 hour scratch area × 100%. The chart below is a statistical analysis of the healing rate, $^{**}p < 0.01$

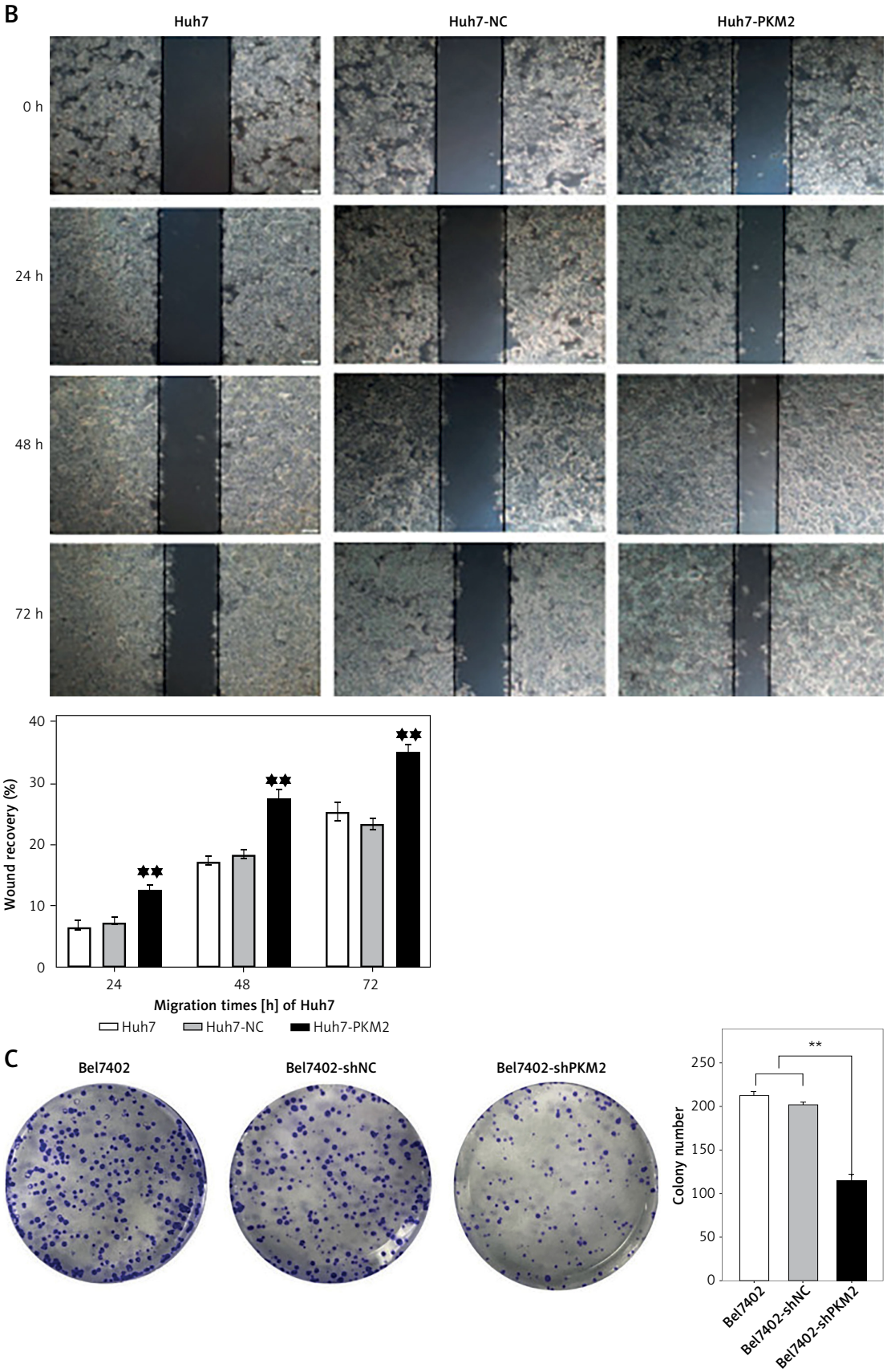

Figure 5. Cont. **B** – Scratch test was used to detect the healing of Huh7 cells groups at 0, 24, 48 and 72 h. The chart below is the statistical analysis of the healing rate, $^{**}p < 0.01$. **C** – The number of clonal formation of cells in Bel7402 groups was detected by plate cloning experiment, and the number of colonies formed in each group was statistically analyzed, $^{**}p < 0.01$

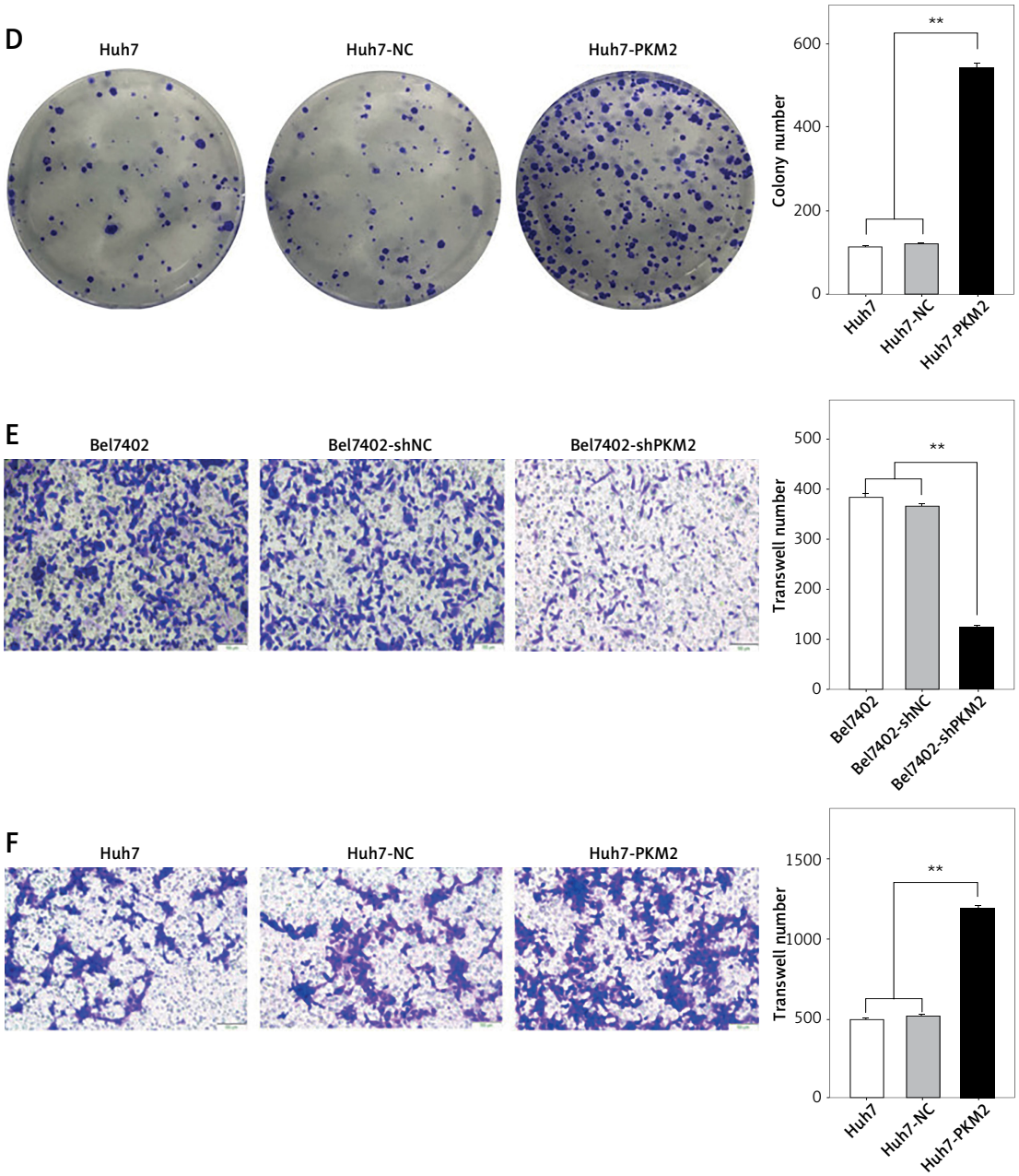

Figure 5. Cont. **D** – The number of colonies formed from Huh7 cells in each group was detected by plate cloning experiment, and the number of colonies formed in each group was statistically analyzed, $^{**}p < 0.01$. **E** – The number of migratory cells in Bel7402 groups at 48 h was detected by Transwell assay. Transwell images were taken with a 10× objective lens with a 100 μm scale bar, and the number of migratory cells in each group was statistically analyzed, $^{**}p < 0.01$. **F** – The number of migratory cells in Huh7 groups at 48 h was detected by Transwell assay, and the number of migratory cells in each group was statistically analyzed, $^{**}p < 0.01$

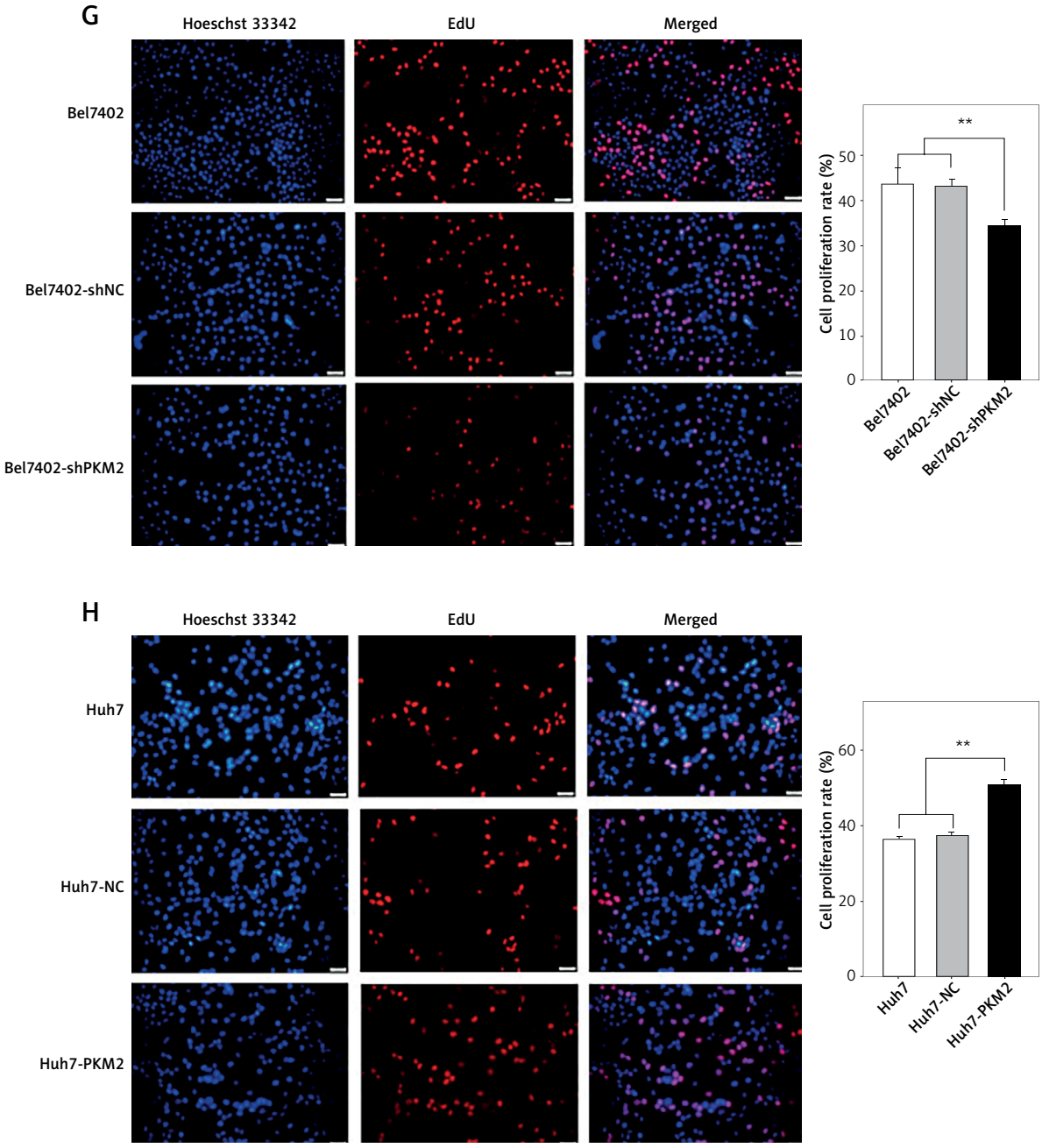

Figure 5. Cont. **G** – EdU test was conducted to detect the number of proliferating cells in the Bel7402 group at 2 h. The nuclei of all cells are in blue, and the nuclei of proliferating cells within 2 h are in red. The fluorescence images were taken with a 20× objective lens with a scale bar of 50 μm. Proliferation rate(%) = (Number of proliferating cells/total cell number in 2 h) × 100%, $^{**}p < 0.01$. **H** – EdU test was conducted to detect the number of proliferating cells of HCC cells in Huh7 groups at 2 h, and the cell proliferation rate of each group was statistically analyzed, $^{**}p < 0.01$. Data are shown as mean ± SD from three independent experiments ($n = 3$). Statistical differences were determined with one-way ANOVA

in Figures 5 A and 5 B. Distant metastasis of malignant tumors usually occurs when a single cell or a small number of cells enter the body fluid to disseminate and colonize other organs. The proliferation ability of a single cell is key to metastasis. Clonal formation experiments reflect cell population dependence and proliferation ability. Through single-cell cloning experiments, we found that the number of colonies formed by Bel7402 cells silenced with PKM2 (Bel7402-shPKM2) was significantly reduced, whereas the number of colonies formed by Huh7 cells overexpressing PKM2 (Huh7-PKM2) was significantly increased. These results indicated that PKM2 knockdown may inhibit clonal formation in HCC cells, and overexpression of PKM2 may increase clonal formation in HCC cells. ImageJ software was used for cell counting, and the number of clones formed was

calculated for statistical analysis. This difference was statistically significant ($p < 0.01$), as shown in Figures 5 C and 5 D.

Collective migration is considered the main type of cancer metastasis and invasion, and in the process of collective migration, propagating cells are connected to each other by adhesion molecules. Compared to single-cell transmission, the collective migration of cancer cells has a higher invasion and metastasis potential. Transwell experiments showed that the number of migratory Bel7402-shPKM2 cells was significantly lower than that in the negative control vector group (Bel7402-shNC) and the control group (Bel7402). However, the number of migratory Huh7-PKM2 cells was significantly higher than that of the negative control vector (Huh7-NC) and control groups (Huh7). These results suggested that PKM2 knockdown may reduce the migratory ability of HCC cells, whereas overexpression of PKM2 may enhance the migratory ability of HCC cells. ImageJ software was used for cell counting, and the number of migratory cells was calculated for statistical analysis; this difference was statistically significant ($p < 0.01$), as shown in Figures 5 E and 5 F. Newly proliferated cells within 2 h were labeled using the EdU cell proliferation assay, and cell proliferation was observed in each group. As shown in Figures 5 G and 5 H, blue represents the nucleus of all cells, and red represents the nucleus of proliferating cells within 2 h. The number of proliferating cells (red) of Bel7402-shPKM2 is significantly reduced, while the number of proliferating cells (red) of Huh7-PKM2 is significantly increased. It has been suggested that silencing PKM2 may inhibit the proliferation of HCC cells and overexpression of PKM2 may promote the proliferation of HCC cells. ImageJ software was used for cell counting, and the cell proliferation rate was calculated for statistical analysis, and the difference was statistically significant ($p < 0.01$). These results indicated that PKM2 was able to promote the migration and proliferation of HCC cells.

PKM2 increases the concentrations of lactic acid, pyruvate, and ATP and glucose consumption in HCC cells

To detect the changes in the concentrations of lactic acid, pyruvate, ATP, and glucose consumption of HCC cells after silencing or overexpression of PKM2, we used a chemical detection kit and performed the operations according to the manufacturer's instructions. The absorbance and RLU values were detected with an enzyme marker and a microplate luminescence detector, respectively, and the corresponding concentrations were calculated according to the formula. As shown in Figure 6 A, compared to the control group (Bel7402) and the negative control vector group (Bel7402-shNC), the levels of lactic acid, pyruvate, ATP, and glucose consumption of cells in the shPKM2 vector group (Bel7402-shPKM2) were reduced to varying degrees. As shown in Figure 6 B, compared to the control group (Huh7) and the negative control vector group (Huh7-NC), the concentrations of lactic acid, pyruvate, ATP, and glucose consumption of cells in the LV-PKM2 group (Huh7-PKM2) were elevated to varying degrees; statistical analysis confirmed that the differences were statistically significant ($p < 0.01$). These results indicated that silencing PKM2 could effectively reduce the concentrations of lactic acid, pyruvate, ATP, and glucose consumption, and weaken the Warburg effect. However, PKM2 overexpression effectively increased the concentrations of lactic acid, pyruvate, ATP, and glucose consumption. These results implied that PKM2 could enhance the Warburg effect in HCC cells.

Lactic acid promotes PD-L1 expression in HCC cells

Lactic acid is the end-product of aerobic glycolysis. To further verify whether glycolysis productions can affect the expression of PD-L1 in HCC cells, we treated Bel7402 cells with a lactic acid concentration of 2.3 mmol/l for 48 h and Huh7 cells at a lactic acid concentration of 1.7 mmol/l for 48 h. The lactic acid concentration used in this study was consistent with that detected using the kit described above in Bel7402 and Huh7 cells. Western blotting was performed to detect the expression of PD-L1 and key glycolytic enzymes. As shown in Figures 7 A and 7 B, after lactic acid treatment of Bel7402 and Huh7 cells, the expression of PD-L1 and the key glycolytic enzymes was significantly increased, and the gray values of the bands were analyzed and found to be statistically significant ($p < 0.01$). These results indicated that lactic acid was able to stimulate the expression of PD-L1 and key glycolytic enzymes in HCC cells.

PKM2 stimulates the expression of PD-L1 in liver cancer cells through the PI3K/Akt/mTOR signaling pathway

The PI3K/Akt/mTOR signaling pathway is closely related to the Warburg effect in cancer cells, and the PI3K/Akt/mTOR signaling pathway has a regulatory effect on PD-L1 expression. Therefore, we speculated that glucose metabolism reprogramming (Warburg effect) could regulate the expression of PD-L1 through the PI3K/Akt/mTOR signaling pathway. Therefore, the PI3K inhibitor Ly294002 was selected to treat Bel7402 and Huh7 cells for 48 h at a concentration of 50 mmol/l. The expression of PD-L1, key glycolysis enzymes and

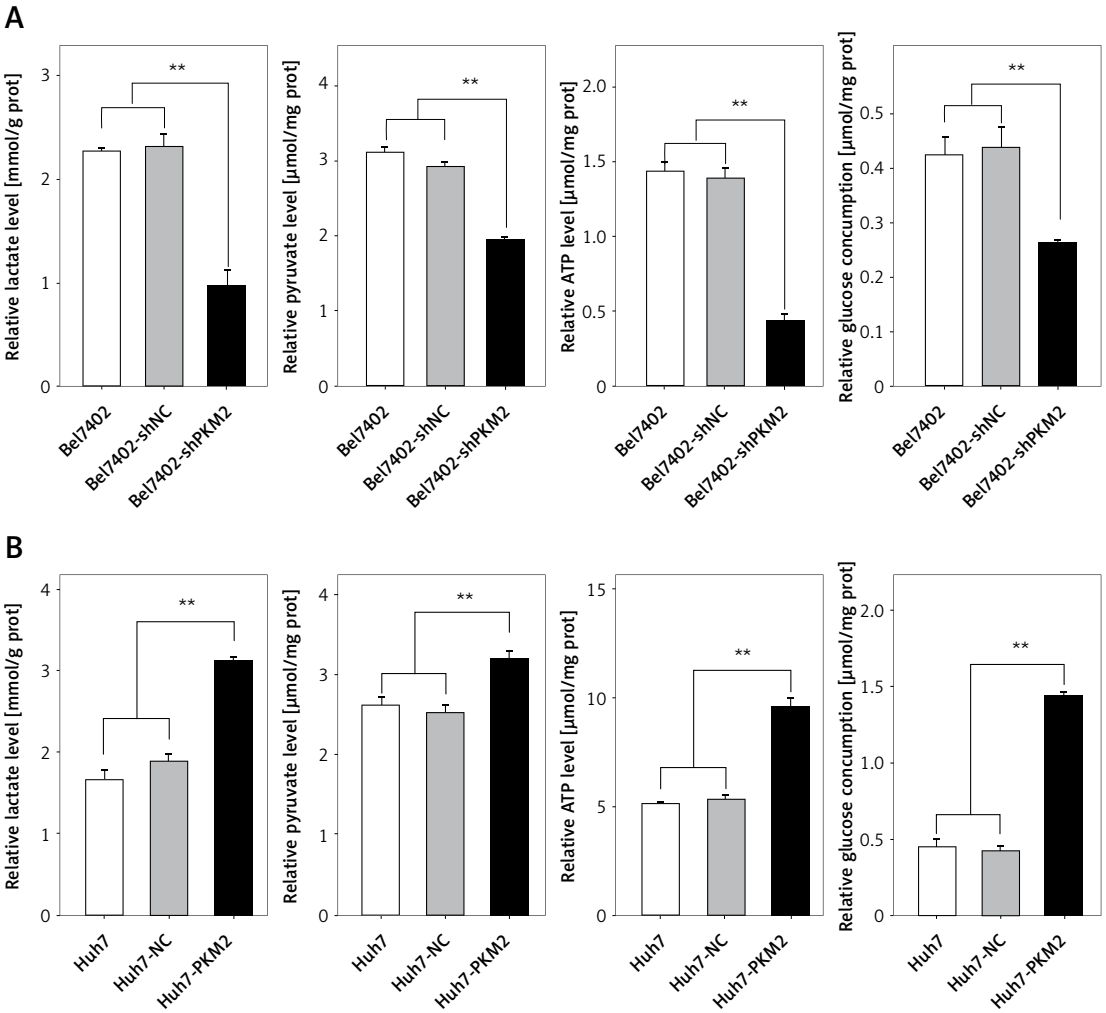

Figure 6. Changes in concentrations of lactic acid, pyruvate, and ATP, and glucose consumption in liver cancer cells were detected by reagent kit. **A** – The changes in the concentrations of lactic acid, pyruvate, and ATP and glucose consumption of cells in Bel7402 groups were detected using the kit, and statistical analysis was performed, $^{**}p < 0.01$. **B** – The changes in concentrations of lactic acid, pyruvate, ATP and glucose consumption of cells in Huh7 groups were detected using a kit, and statistical analysis was performed, $^{**}p < 0.01$. Data are shown as mean ± SD from three independent experiments ($n = 3$). Statistical differences were determined with one-way ANOVA

PI3K-related pathway proteins was detected using Western blotting. As shown in Figure 8 A, Bel7402 cells treated with Ly294002 showed the same effect as that of Bel7402-shPKM2, which inhibited the expression of PKM2. The expression levels of PD-L1, PKM2, phosphorylated-PKM2 (p-PKM2), lactate dehydrogenase A (LDHA), phosphorylated-LDHA (p-LDHA), HK2, phosphofructokinase 1 (PFK1), HIF-1α, and phosphorylated-Akt (p-Akt) decreased significantly, suggesting that silencing the expression of PKM2 may inhibit the expression of PD-L1 by blocking the PI3K/Akt/mTOR signaling pathway. The gray values of the strips were analyzed and found to be statistically significant ($p < 0.01$). As shown in Figure 8 B, compared to Huh7 and Huh7-NC, the protein expression levels of PD-L1, PKM2, p-PKM2, LDHA, p-LDHA, HK2, PFK1, HIF-1α, and p-Akt in Huh7-PKM2 cells were significantly elevated. However, the expression levels of PD-L1, PKM2, p-PKM2, LDHA, p-LDHA, HK2, PFK1, HIF-1α, and p-Akt were significantly decreased, whereas Huh7-PKM2 cells were treated with Ly294002. The gray values of the strips were analyzed and found to be statistically significant ($p < 0.01$). These results indicated that PKM2 may promote the expression of PD-L1 and Warburg effect-related enzymes by activating the PI3K/Akt/mTOR signaling pathway. Thus, it was verified that PKM2 regulates the expression of PD-L1 through the PI3K/Akt/mTOR signaling pathway, and PKM2 also stimulates the expression of other enzymes that promote glucose metabolic reprogramming in HCC cells.

Discussion

HCC is the most common primary liver cancer, and usually develops in the context of chronic

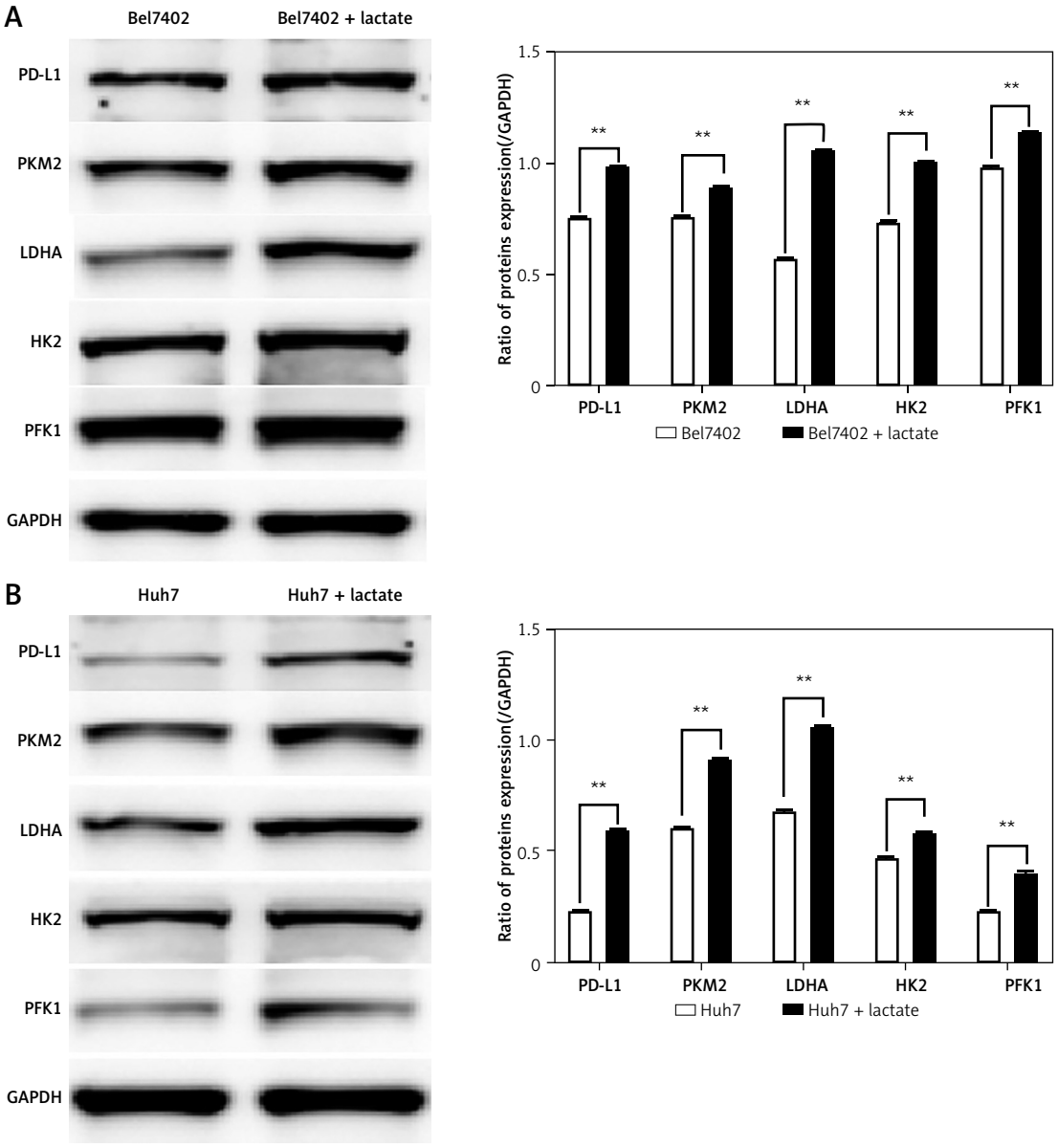

Figure 7. The effect of lactic acid on expression of PD-L1 and key glycolytic enzymes in HCC cells. **A** – After lactic acid treatment for 72 h, Western blotting was applied to detect the changes of PD-L1 and key glycolytic enzyme in Bel7402 cells. The amount of protein samples per well was 20–50 μg. The chart on the right shows the statistical diagram of bands after gray scale analysis for each group, $^{**}p < 0.01$. **B** – After lactic acid treatment of Huh7 cells for 72 h, Western blotting was used to detect the changes of PD-L1 and glycolytic enzyme in Huh7 cells, and the protein sample amount per well was 20–50 μg. The chart on the right is the statistical graph of bands after gray scale analysis for each group, $^{**}p < 0.01$. Data are shown as mean ± SD from three independent experiments ($n = 3$). *P*-values were calculated using unpaired two-sided Student's *t* test

liver disease. Hepatitis virus infection, alcoholic liver disease, and non-alcoholic fatty liver disease are the main causes. It is an aggressive disease with poor prognosis [34], and the incidence of this disease is increasing every year, with a higher incidence in developing countries. The prognosis of liver cancer is very poor; only 5–15% of early stage patients are eligible for surgical resection, and the treatment options for advanced stages are mainly arterial chemoembolization and oral sorafenib, while long-term oral sorafenib is prone to drug resistance [35]. HCC therapy has recently introduced immunotherapy strategies that selectively target tumor cells by inducing or enhancing existing tumor-specific immune responses and immune checkpoint pathway inhibitors. For example, anti-cytotoxic T lymphocyte-associated antique-4 (CTLA-4) antibodies and PD-1/PD-L1 inhibitors have shown good therapeutic effects [36, 37]. The combination of PD-1 and PD-L1 is an important immune checkpoint and a major mechanism of immunosuppression in the tumor micro-

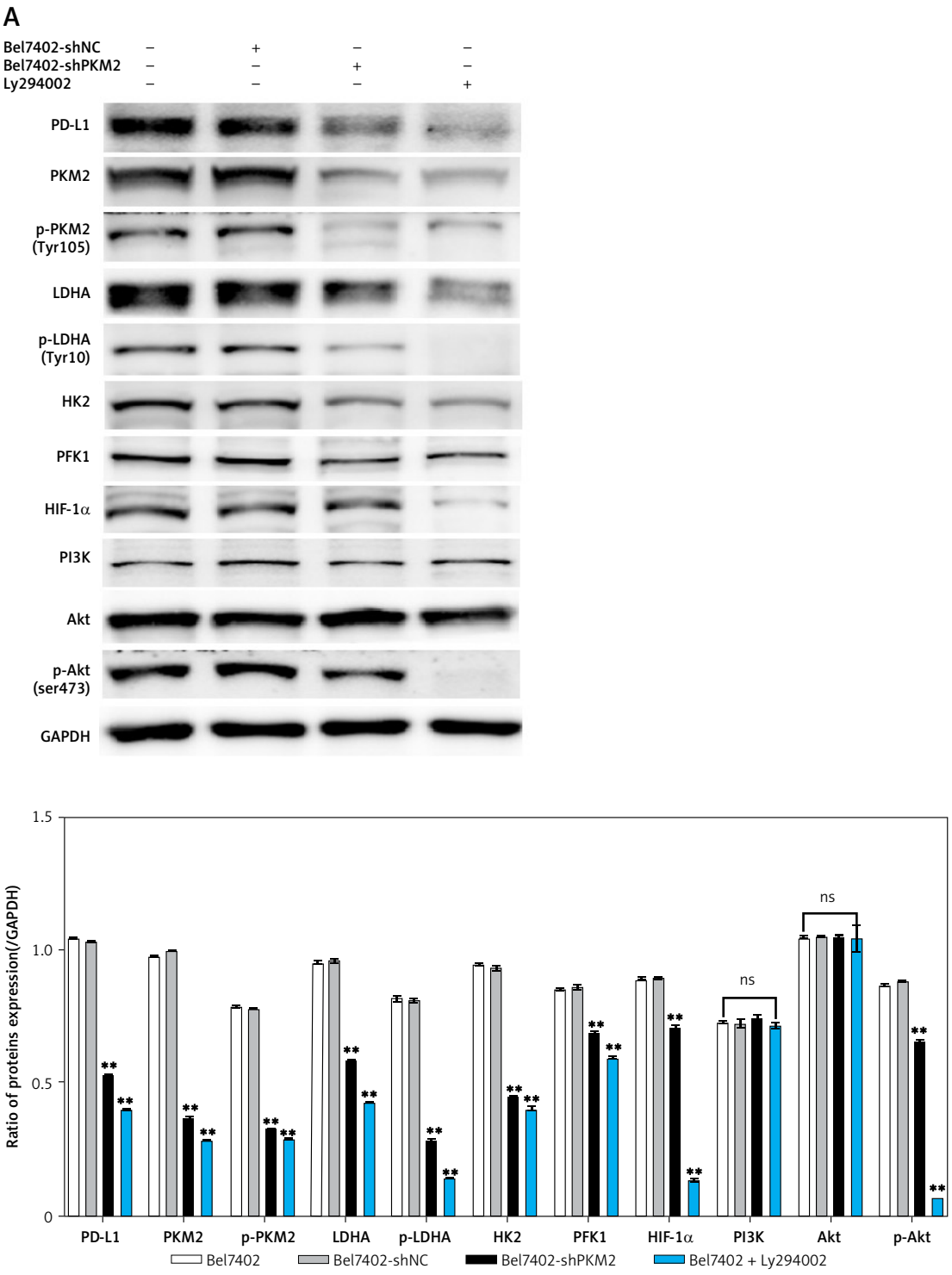

Figure 8. Effects of PI3K/Akt signaling pathway on PKM2 regulating the expression of PD-L1 and other key glycolytic enzymes. **A** – Western blotting detected the expression of PD-L1, key glycolytic enzymes, and PI3K/Akt signaling pathway-related proteins in Bel7402, Bel7402-shNC, and Bel7402-shPKM2 cells before and after treatment with Ly294002 for 48 h. The amount of protein samples per well was 20–50 μg. The chart on the right showed the statistical map of each group after gray scale analysis, $^{**}p < 0.01$

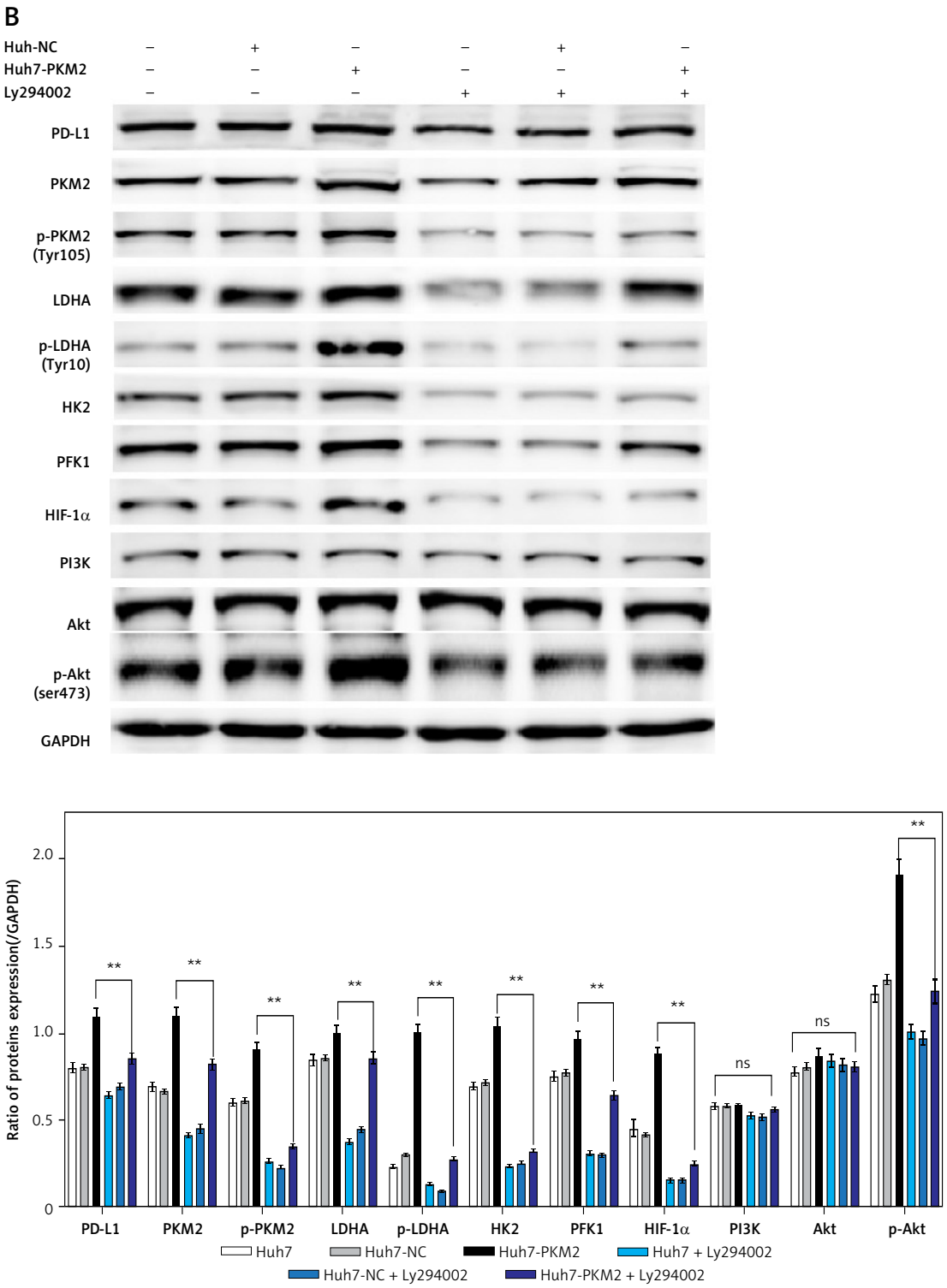

Figure 8. Cont. **B** – Western blotting was used to detect the expression of PD-L1, key glycolytic enzymes, and PI3K/Akt signaling pathway-related proteins in Huh7, Huh7-NC, Huh7-PKM2 cells before and after treatment with Ly294002 for 48 h. The protein sample amount per pore was 20–50 μg. The chart on the right is the statistical graph of each group of strips after gray level analysis, $^{**}p < 0.01$. Data are shown as mean ± SD from three independent experiments ($n = 3$). Statistical differences were determined with one-way ANOVA

environment. Gao *et al*. [38] demonstrated that increased expression of PD-L1 in HCC is positively correlated with tumor aggressiveness and the risk of postoperative recurrence. Pazgan-Simon *et al*. found that high levels of chemerin in the serum of HCC patients promote immune escape of liver cancer cells [39], suggesting that PD-L1 in serum may also affect the immune surveillance of liver cancer cells. Therefore, PD-L1 can be used as a target and biomarker for HCC immunotherapy. Although immunotherapy has brought great hope and new opportunities for the treatment of liver cancer patients, some HCC patients have little positive clinical response to this treatment, so there is an urgent need for combination therapy or personalized treatment options for anti-tumor responses [40]. Currently, a variety of combination therapies have been reported, such as combination therapy with polyinosinic-polycytidylic acid (polyIC) and PD-L1 antibody [41], and combination therapy with CTLA-4 and PD-L1 inhibitors [42]. Radiotherapy is a combination of immunotherapy and adoptive cell therapy (ACT) combined with ICIs [43].

The liver plays a key role in maintaining blood sugar levels through glycogenolysis and gluconeogenesis, and glucose utilization (glycolysis) mainly occurs after meals. One of the characteristics of tumor cells is that glucose metabolism changes during proliferation and growth to meet the high energy requirements [44]. As one of the key enzymes involved in glycolysis, PKM2 is widely expressed during embryogenesis, regeneration, and cancer. Pyruvate kinase activity is very important for cells with active proliferation [45], and PKM2 plays a regulatory role in the tumor microenvironment [46]. There were obvious differences in glucose metabolism between tumor and normal cells. In view of this feature of tumor cells, some therapeutic drugs targeting tumor metabolism have shown significant cancer cell toxicity in preclinical studies [47]. However, there are few reports on the correlation between glucose metabolism and PD-L1 expression in liver cancer. To explore the correlation between glucose metabolic reprogramming (Warburg effect) and PD-L1 expression in liver cancer cells, we first analyzed the correlation between PD-L1 and PKM2 using a biological information database and found that it was positively correlated, and PD-L1 was associated with the PI3K/Akt signaling pathway to some extent. Immunohistochemistry and Western blotting were used to detect the expression of PD-L1 and PKM2 in liver cancer tissues of 30 patients with HCC. The results showed that the expression of PD-L1 and PKM2 was significantly higher in cancer tissues than that in paired para-cancerous tissues, and their expression levels were positively correlated. This suggests that PD-L1 and PKM2 expression levels are correlated with liver cancer.

In the *in vitro* experiments, we first infected Bel7402 cells with lentivirus-shPKM2 (LV-shPKM2) and constructed PKM2 silencing cell lines. To observe the effect of PKM2 knockdown on the malignant biological behaviors of HCC cells, we found that the healing ability, colony formation, migration, and proliferation ability of HCC cells were significantly decreased after PKM2 knockdown. The results of the kit detection showed that the concentrations of lactic acid, pyruvate, and ATP, and glucose consumption also significantly decreased after silencing the expression of PKM2. These results indicate that silencing PKM2 expression weakens the Warburg effect and inhibits the malignant behaviors of HCC cells. Simultaneously, we infected Huh7 cells with a PKM2-expressing lentivirus and constructed stable cell lines overexpressing PKM2. In order to observe the role of PKM2 overexpression in the malignant behaviors of liver cancer cells, we conducted a series of experiments. The results showed that after overexpression of PKM2, the healing ability of HCC cells was enhanced, the number of colonies was increased, and the migration and proliferation abilities were stimulated. After PKM2 overexpression, the levels of lactic acid, pyruvate, and ATP in Huh7 cells were increased, and glucose consumption was promoted. These results indicated that overexpression of PKM2 could enhance the Warburg effect and thus stimulate the malignant behaviors of HCC cells. In the present study, the localization of PD-L1 in HCC cells was observed using laser confocal microscopy and cellular immunofluorescence assays. It was found that PD-L1 was mainly located in the cytoplasm and cell membrane, with low expression in the nucleus. After silencing PKM2 in Bel7402 cells, the red brightness of PD-L1 significantly decreased. In contrast, after PKM2 overexpression in Huh7 cells, the red color of PD-L1 was significantly enhanced. These results indicated that PKM2 has a regulatory effect on PD-L1 expression. The detection kit results showed that the levels of lactic acid, pyruvate, and ATP and glucose consumption decreased after inhibition of expression of PKM2 by RNA interference, whereas the levels of lactic acid, pyruvate, and ATP and glucose consumption increased after PKM2 overexpression. It has been suggested that the expression level of PKM2 is indeed related to the strength of the Warburg effect.

In addition to PKM2, other key enzymes are involved in glycolysis to regulate the glucose metabolism. Hexokinase (HK) is the first rate-limiting enzyme in glycolysis that phosphorylates glucose to glucose-6-phosphate (G-6-P). HK belongs to a ubiquitous family of extracellular phosphorylases. HK2 is the most active isoenzyme in this fam-

ily [48]. Previous reports have shown that HK2 is often upregulated in tumor cells and is associated with poor patient prognosis [49]. Li *et al*. [50] used CRISPR/Cas9 *in vivo* to screen metabolic genes that determine tumorigenicity of HCC and found that HK2 expression was elevated in liver cancer. HK2 is highly expressed in liver cancer stem cells (CSC) and is essential for maintaining self-renewal and tumor spread *in vivo*. Phosphofructokinase-1 (PFK1) is an important rate-limiting enzyme that regulates glycolysis, and fructose-2,6-diphosphate is the strongest allosteric activator of PFK1 [51]. PFK1 and its product fructose-1,6-diphosphate (F-1,6-BP) can activate PI3K/AKT and YAP/TAZ through independent mechanisms, and in turn, PI3K/AKT and YAP/TAZ can promote PFK1 and glycolysis in a feedback loop [52]. LDHA catalyzes the conversion of pyruvate to lactic acid, and plays a key role in the regulation of glycolysis. This is usually indicated by the upregulation of LDHA in cancer cells. Tyrosine phosphorylation of LDHA can promote cancer cell metabolism and affect mitochondrial physiology, whereas downregulation of LDHA can inhibit the growth and metastasis of mouse liver cancer cells [53]. HCC cells were treated with lactic acid, and Western blotting experiments showed that the expression of PD-L1 and key glycolytic enzymes PKM2, LDHA, HK2, and PFK1 increased, which proved that lactic acid could promote the expression of PD-L1. To further explore how the Warburg effect regulates the expression of PD-L1, Western blotting experiments were conducted to detect the effect of PKM2 on the expression of PD-L1. The results showed that in Bel7402 cells, while silencing the expression of PKM2, the protein expression of PD-L1 and other key glycolytic enzymes decreased to varying degrees. In contrast, the protein expression of PD-L1 and other key glycolytic enzymes significantly increased in Huh7 cells while overexpressing PKM2. These results indicated that the Warburg effect can stimulate the expression of PD-L1 in HCC cells.

The PI3K/Akt/mTOR signaling pathway is important for cell growth and survival. Numerous experiments have shown that the PI3K/Akt/mTOR signaling pathway is stably activated in liver cancer cells [54] and is closely related to glucose metabolism in tumor cells. Akt enhances glucose uptake by promoting the plasma membrane localization of glucose transporter1 (Glut1). Akt activation enhances the activity of key glycolytic enzymes such as HK2 and PFK1. The PI3K/Akt/mTOR signaling pathway also promotes aerobic glycolysis by controlling downstream transcription factors, and the PI3K/Akt/mTOR signaling pathway can regulate the expression of hypoxia-inducible factor-1α (HIF-1α). HIF-1α is involved in glucose metabolism and angiogenesis [5, 33]. As tumors exist in an inherently stressful environment, this pathway plays a crucial role in cancer. Activation of the PI3K/Akt/mTOR signaling pathway may lead to cell growth disorders. Ultimately, this leads to competitive growth, enhanced metastasis, angiogenesis, and resistance to treatment [56]. The PI3K/Akt/mTOR signaling pathway is often abnormally activated in human cancers owing to dysregulation of different signaling pathway components at the DNA level (including gene amplification, deletion, mutation, and fusion), RNA (transcription and post-transcriptional regulation), and proteins (including protein stability control and post-translational modification) [57]. Activated PI3K phosphorylates phosphatidylinositol-4,5-bisphosphate (PIP2) and converts it into phosphatidylinositol-3,4,5-trisphosphate (PIP3). Phosphatidylinositol 3,4,5-triphosphate (PIP3) recruits 3-phosphoinositide dependent protein kinase 1 (PDK1) and Akt to the plasma membrane, and PDK1 phosphorylates Akt at Thr380 to activate part of it [58]. Bamodu *et al*. [59] found that PDK1 is an independent driver of the PI3K/Akt/mTOR signaling pathway, and its abnormal expression is characteristic of poorly differentiated HCC cells. The decrease in PDK1 expression may inactivate the PI3K/Akt/mTOR signaling pathway and render invasive HCC cells sensitive to radiotherapy. Spalt-like transcription factor 4 (SALL4) is an important player in the early and middle stages of fetal liver development, as it is one of the few embryonic stem cell (ESC) genes that are in contact with cancer cells. SALL4 activates the PI3K/AKT signaling pathway by targeting PTEN, thereby promoting the migration, invasion, and proliferation of liver cancer cells [60]. Evidence showed that blocking the PI3K/AKT signaling pathway can counteract drug treatment tolerance and immune escape of cancer cells [61], indicating that the PI3K/AKT signaling pathway plays a key role in the immune escape in liver cancer cells. In the present study, after treating HCC cells with Ly294002, a PI3K/Akt signaling pathway inhibitor, Western blotting was used to detect changes in PD-L1, key glycolytic enzymes, and PI3K/Akt signaling pathway-related proteins. The expression levels of PD-L1, PKM2, p-PKM2, LDHA, p-LDHA, HK2, PFK1, HIF-1α, and p-Akt significantly decreased. These results prove that the Warburg effect may regulate the expression of PD-L1 in HCC cells through the PI3K/Akt signaling pathway. Recently, studies have shown that lactic acid could inhibit the function of P53 and promote the occurrence of tumors [62], suggesting that lactic acid, a product of glucose metabolism reprogramming, can promote the malignant behaviors of liver cancer cells. Although the role of PD-L1 in the process of immune escape of cancer

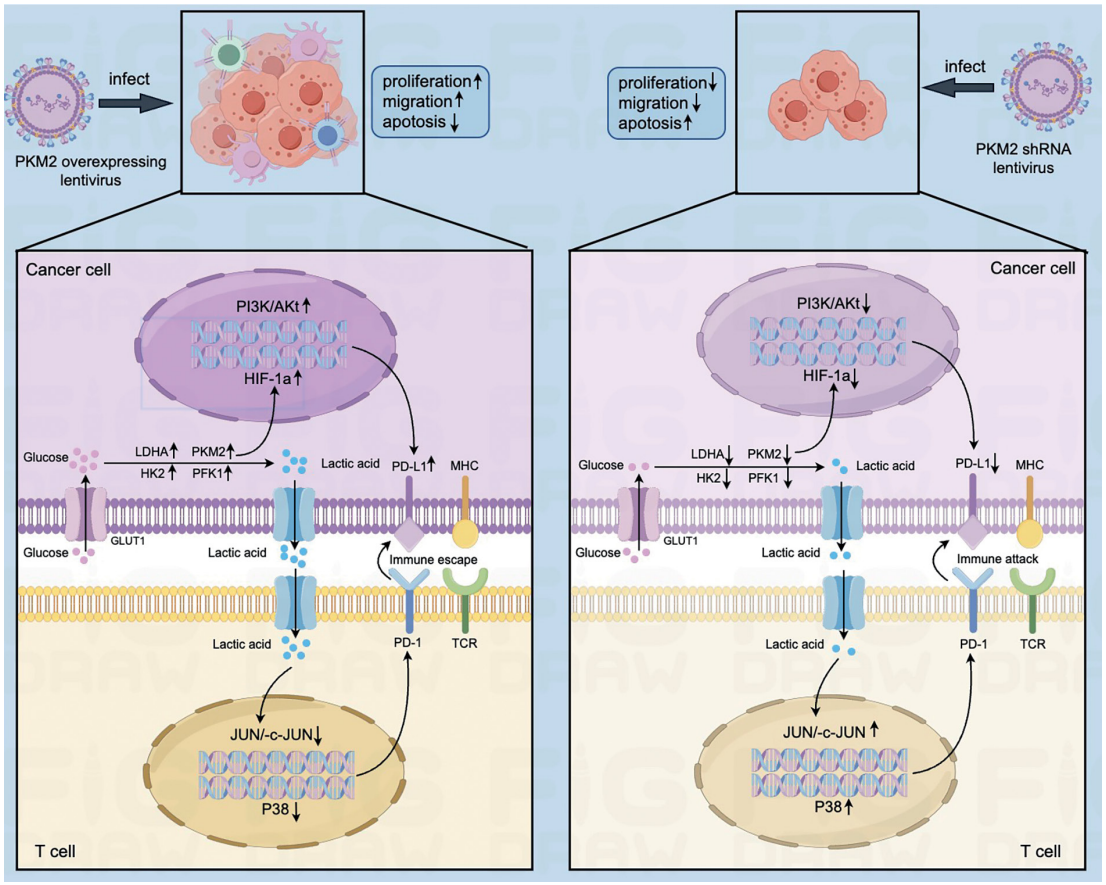

Figure 9. Schematic diagram of liver cancer cells expressing PD-L1 and promoting immune escape induced by lactic acid, a product of glucose metabolic reprogramming

cells needs to be further explored, the Warburg effect induced by PKM2 can increase the energy synthesis of cancer cells [63, 64], suggesting that the regulation of PD-L1 expression by PKM2 plays an important role in the immune escape of liver cancer cells. Figure 9 summarizes the mechanism by which lactic acid, the product of glucose metabolic reprogramming, induces liver cancer cells to express PD-L1 and promote immune escape.

In conclusion, we preliminarily demonstrated that the expression of PKM2 and PD-L1 is positively correlated in liver cancer tissues, and that PKM2, a key enzyme regulating the Warburg effect, may regulate the expression of PD-L1 in liver cancer cells through the PI3K/Akt signaling pathway. This study revealed the relationship between glucose metabolic reprogramming and PD-L1, as well as the signaling pathways that may be involved, providing new ideas for immunotherapy in liver cancer. Combining targeted PKM2 therapy with immunotherapy may have synergistic effects and provide new treatment options for patients with liver cancer. However, because the processes of glucose metabolic reprogramming and the immune system are relatively complex, other molecular mechanisms may be involved. The study results proved that PKM2 is a pivotal factor in promoting the expression of PD-L1 and stimulating the malignant behaviors of HCC cells, and the molecular mechanism may be involved in activating the PI3K/Akt signaling pathway. Targeting PKM2 is a promising strategy for liver cancer treatment.

Acknowledgments

Qiuyue Zhang, Kailin Huang, and Junnv Xu have contributed equally to this work and share co-first authorship.

Funding

This study was supported by the National Natural Science Foundation of China (Nos. 82460602, 82060514 and 81960519) and the Research Project of Take Off the Proclamation and Leadership of the Hainan Medical College Natural Science Foundation (No. JBGS202106), Natural Science Foundation of Hainan Province (No. 822QN311, 820QN403), Nanhai Junior Talent Program of the Hainan Provincial Health Commission (No. NHXX-WJW-2023014), the Hainan Medical University Talent Launch Fund (No. XRC220017), Hainan Province Graduate Student Innovation

Project (No. Qhyb2023-175), and Hainan Provincial Science and Technology Special Fund (No. ZDYF2021SHF222).

Ethical approval

This study was approved by the Academic Ethics Committee of the Hainan Medical University. We confirm that all methods were performed in accordance with the relevant guidelines and regulations by including a statement in the Methods section regarding the effect.

Conflict of interest

The authors declare no conflict of interest.

References

1. Llovet JM, Kelley RK, Villanueva A, et al. Hepatocellular carcinoma. Nat Rev Dis Primers 2021; 7: 6.
2. Llovet JM, Zucman-Rossi J, Pikarsky E, et al. Hepatocellular carcinoma. Nat Rev Dis Primers 2016; 2: 16018.
3. Ouyang T, Kan X, Zheng C. Immune checkpoint inhibitors for advanced hepatocellular carcinoma: monotherapies and combined therapies. Front Oncol 2022; 12: 898964.
4. Chen Y, Hu H, Yuan X, Fan X, Zhang C. Advances in immune checkpoint inhibitors for advanced hepatocellular carcinoma. Front Immunol 2022; 13: 896752.
5. Han Y, Liu D, Li L. PD-1/PD-L1 pathway: current researches in cancer. Am J Cancer Res 2020; 10: 727-42.
6. Cha JH, Chan LC, Li CW, Hsu JL, Hung MC. Mechanisms controlling PD-L1 expression in cancer. Mol Cell 2019; 76: 359-70.
7. Xu F, Jin T, Zhu Y, Dai C. Immune checkpoint therapy in liver cancer. J Exp Clin Cancer Res 2018; 37: 110.
8. Tang Q, Chen Y, Li X, et al. The role of PD-1/PD-L1 and application of immune-checkpoint inhibitors in human cancers. Front Immunol 2022; 13: 964442..
9. Xia P, Zhang H, Lu H, et al. METTL5 stabilizes c-Myc by facilitating USP5 translation to reprogram glucose metabolism and promote hepatocellular carcinoma progression. Cancer Commun (Lond) 2023; 43: 338-64.
10. Zhou Q, Yin Y, Yu M, et al. GTPBP4 promotes hepatocellular carcinoma progression and metastasis via the PKM2 dependent glucose metabolism. Redox Biol 2022; 56: 102458.
11. Peñuelas-Haro I, Espinosa-Sotelo R, Crosas-Molist E, et al. The NADPH oxidase NOX4 regulates redox and metabolic homeostasis preventing HCC progression. Hepatology 2023; 78: 416-33.
12. Du D, Liu C, Qin M, et al. Metabolic dysregulation and emerging therapeutical targets for hepatocellular carcinoma. Acta Pharm Sin B 2022; 12: 558-80.
13. Liberti MV, Locasale JW. The Warburg effect: How does it benefit cancer cells? Trends Biochem Sci 2016; 41: 211-8.
14. Gatenby RA, Gawlinski ET. A reaction-diffusion model of cancer invasion. Cancer Res 1996; 56: 5745-53.
15. Estrella V, Chen T, Lloyd M, et al. Acidity generated by the tumor microenvironment drives local invasion. Cancer Res 2013; 73: 1524-35.
16. Chang CH, Qiu J, O'Sullivan D, et al. Metabolic competition in the tumor microenvironment is a driver of cancer progression. Cell 2015; 162: 1229-41.
17. Wiese EK, Hitosugi T. Tyrosine kinase signaling in cancer metabolism: PKM2 paradox in the Warburg effect. Front Cell Dev Biol 2018; 6: 79.
18. Luo W, Semenza GL. Emerging roles of PKM2 in cell metabolism and cancer progression. Trends Endocrinol Metab 2012; 23: 560-6.
19. Ishfaq M, Bashir N, Riaz SK, et al. Expression of HK2, PKM2, and PFKM is associated with metastasis and late disease onset in breast cancer patients. Genes (Basel) 2022; 13: 549.
20. Azoitei N, Becher A, Steinestel K, et al. PKM2 promotes tumor angiogenesis by regulating HIF-1α through NF-κB activation. Mol Cancer 2016; 15: 3.
21. Wang Y, Hao F, Nan Y, et al. PKM2 inhibitor Shikonin overcomes the cisplatin resistance in bladder cancer by inducing necroptosis. Int J Biol Sci 2018; 14: 1883-91.
22. Li TE, Wang S, Shen XT, et al. PKM2 drives hepatocellular carcinoma progression by inducing immunosuppressive microenvironment. Front Immunol 2020; 11: 589997.
23. Zhang Z, Deng X, Liu Y, Liu Y, Sun L, Chen F. PKM2, function and expression and regulation. Cell Biosci 2019; 9: 52.
24. Yang W, Xia Y, Hawke D, et al. PKM2 phosphorylates histone H3 and promotes gene transcription and tumorigenesis. Cell 2012; 150: 685-96.
25. Xu F, Na L, Li Y, Chen L. Roles of the PI3K/AKT/mTOR signalling pathways in neurodegenerative diseases and tumours. Cell Biosci 2020; 10: 54.
26. Tang X, Yang J, Shi A, et al. CD155 cooperates with PD-1/PD-L1 to promote proliferation of esophageal squamous cancer cells via PI3K/Akt and MAPK signaling pathways. Cancers(Basel) 2022; 14: 5610.
27. Wang F, Yang L, Xiao M, et al. PD-L1 regulates cell proliferation and apoptosis in acute myeloid leukemia by activating PI3K-AKT signaling pathway. Sci Rep 2022; 12: 11444.
28. Piao W, Li L, Saxena V, et al. PD-L1 signaling selectively regulates T cell lymphatic transendothelial migration. Nat Commun 2022; 13: 2176.
29. Quan Z, Yang Y, Zheng H, et al. Clinical implications of the interaction between PD-1/PD-L1 and PI3K/AKT/mTOR pathway in progression and treatment of non-small cell lung cancer. J Cancer 2022; 13: 3434-43.
30. Atefi M, Avramis E, Lassen A, et al. Effects of MAPK and PI3K pathways on PD-L1 expression in melanoma. Clin Cancer Res 2014; 20: 3446-57.
31. Parsa AT, Waldron JS, Panner A, et al. Loss of tumor suppressor PTEN function increases B7-H1 expression and immunoresistance in glioma. Nat Med 2007; 13: 84-8.
32. Gao Y, Yang J, Cai Y, et al. IFN-γ-mediated inhibition of lung cancer correlates with PD-L1 expression and is regulated by PI3K-AKT signaling. Int J Cancer 2018; 143: 931-43.
33. Hoxhaj G, Manning BD. The PI3K-AKT network at the interface of oncogenic signalling and cancer metabolism. Nat Rev Cancer 2020; 20: 74-88.
34. Craig AJ, von Felden J, Garcia-Lezana T, Sarcognato S, Villanueva A. Tumour evolution in hepatocellular carcinoma. Nat Rev Gastroenterol Hepatol 2020; 17: 139-52.
35. Anwanwan D, Singh SK, Singh S, Saikam V, Singh R. Challenges in liver cancer and possible treatment approaches. Biochim Biophys Acta Rev Cancer 2020; 1873: 188314.
36. Liu CY, Chen KF, Chen PJ. Treatment of liver cancer. Cold Spring Harb Perspect Med 2015; 5: a021535.
37. Sangro B, Sarobe P, Hervás-Stubbs S, Melero I. Advances in immunotherapy for hepatocellular carcinoma. Nat Rev Gastroenterol Hepatol 2021; 18: 525-43.

38. Gao Q, Wang XY, Qiu SJ, et al. Overexpression of PD-L1 significantly associates with tumor aggressiveness and postoperative recurrence in human hepatocellular carcinoma. Clin Cancer Res 2009; 15: 971-9.
39. Pazgan-Simon M, Szymanek-Pasternal A, Górka-Dynysiewicz J, et al. Serum chemerin level in patients with liver cirrhosis and primary and multifocal hepatocellular carcinoma with consideration of insulin level. Arch Med Sci 2024; 20: 1504-10.
40. Fu Y, Liu S, Zeng S, Shen H. From bench to bed: the tumor immune microenvironment and current immunotherapeutic strategies for hepatocellular carcinoma. J Exp Clin Cancer Res 2019; 38: 396.
41. Wen L, Xin B, Wu P, et al. An efficient combination immunotherapy for primary liver cancer by harmonized activation of innate and adaptive immunity in mice. Hepatology 2019; 69: 2518-32.
42. Yap TA, Parkes EE, Peng W, Moyers JT, Curran MA, Tawbi HA. Development of immunotherapy combination strategies in cancer. Cancer Discov 2021; 11: 1368-97.
43. Zhu S, Zhang T, Zheng L, et al. Combination strategies to maximize the benefits of cancer immunotherapy. J Hematol Oncol 2021; 14: 156.
44. Satriano L, Lewinska M, Rodrigues PM, Banales JM, Andersen JB. Metabolic rearrangements in primary liver cancers: cause and consequences. Nat Rev Gastroenterol Hepatol 2019; 16: 748-66.
45. Dayton TL, Jacks T, Vander Heiden MG. PKM2, cancer metabolism, and the road ahead. EMBO Rep 2016; 17: 1721-30.
46. Zhu S, Guo Y, Zhang X, et al. Pyruvate kinase M2 (PKM2) in cancer and cancer therapeutics. Cancer Lett 2021; 503: 240-8.
47. Madhok BM, Yeluri S, Perry SL, Hughes TA, Jayne DG. Targeting glucose metabolism: an emerging concept for anticancer therapy. Am J Clin Oncol 2011; 34: 628-35.
48. Ciscato F, Ferrone L, Masgras I, Laquatra C, Rasola A. Hexokinase 2 in cancer: a prima donna playing multiple characters. Int J Mol Sci 2021; 22: 4716.
49. Jiao L, Zhang HL, Li DD, et al. Regulation of glycolytic metabolism by autophagy in liver cancer involves selective autophagic degradation of HK2(hexokinase 2). Autophagy 2018; 14: 671-84.
50. Li H, Song J, He Y, et al. CRISPR/Cas9 screens reveal that Hexokinase 2 enhances cancer stemness and tumorigenicity by activating the ACSL4-fatty acid β-oxidation pathway. Adv Sci Weinh 2022; 9: e2105126.
51. Bartrons R, Simon-Molas H, Rodríguez-García A, et al. Fructose 2,6-bisphosphate in cancer cell metabolism. Front Oncol 2018; 8: 331.
52. Simula L, Alifano M, Icard P. How phosphofructokinase-1 promotes PI3K and YAP/TAZ in cancer: therapeutic perspectives. Cancers (Basel) 2022; 14: 2478.
53. Jin L, Chun J, Pan C, et al. Phosphorylation-mediated activation of LDHA promotes cancer cell invasion and tumour metastasis. Oncogene 2017; 36: 3797-806.
54. Pu Z, Duda DG, Zhu Y, et al. VCP interaction with HMGB1 promotes hepatocellular carcinoma progression by activating the PI3K/AKT/mTOR pathway. J Transl Med 2022; 20: 212.
55. Hwang SJ, Cho SH, Bang HJ, Hong JH, Kim KH, Lee HJ. 1,8-Dihydroxy-3-methoxy-anthraquinone inhibits tumor angiogenesis through HIF-1alpha downregulation. Biochem Pharmacol 2024; 220: 115972.
56. Glaviano A, Foo ASC, Lam HY, et al. PI3K/AKT/mTOR signaling transduction pathway and targeted therapies in cancer. Mol Cancer 2023; 22: 138.
57. Yu L, Wei J, Liu P. Attacking the PI3K/Akt/mTOR signaling pathway for targeted therapeutic treatment in human cancer. Semin Cancer Biol 2022; 85: 69-94.
58. Sun EJ, Wankell M, Palamuthusingam P, McFarlane C, Hebbard L. Targeting the PI3K/Akt/mTOR pathway in hepatocellular carcinoma. Biomedicines 2021; 9: 1639.
59. Bamodu OA, Chang HL, Ong JR, Lee WH, Yeh CT, Tsai JT. Elevated PDK1 expression drives PI3K/AKT/MTOR signaling promotes radiation-resistant and dedifferentiated phenotype of hepatocellular carcinoma. Cells 2020; 9: 746.
60. Tang Z, Zhao P, Zhang W, Zhang Q, Zhao M, Tan H. SALL4 activates PI3K/AKT signaling pathway through targeting PTEN, thus facilitating migration, invasion and proliferation of hepatocellular carcinoma cells. Aging (Albany NY) 2022; 14: 10081-92.
61. Hong T, Dong D, Li J, Wang L. PARP9 knockdown confers protection against chemoresistance and immune escape of breast cancer cells by blocking the PI3K/AKT pathway. Arch Med Sci 2023; 20: 1228-48.
62. Zong Z, Xie F, Wang S, et al. Alanyl-tRNA synthetase, AARS1, is a lactate sensor and lactyltransferase that lactylates p53 and contributes to tumorigenesis. Cell 2024; 187: 2375-92.
63. Song H, Chen L, Pan X, et al. Targeting tumor monocyte-intrinsic PD-L1 by rewiring STING signaling and enhancing STING agonist therapy. Cancer Cell 2025; 43: 503-18.e10.
64. Zhang J, Ouyang F, Gao A, et al. ESM1 enhances fatty acid synthesis and vascular mimicry in ovarian cancer by utilizing the PKM2-dependent warburg effect within the hypoxic tumor microenvironment. Mol Cancer 2024; 23: 94.